DIRECT BED SHEAR STRESS MEASUREMENTS IN BORE-DRIVEN SWASH

M.P. Barnes[1]*, T. O'Donoghue[2], J.M. Alsina[1] and T. E. Baldock[1]

[1] Department of Civil Engineering, University of Queensland

St Lucia, Queensland 4072, Australia.

[2] School of Engineering, University of Aberdeen, Aberdeen AB24 3UE, UK.

Abstract

Direct measurements of bed shear in the swash zone are presented. The data were obtained using a shear plate in medium and large scale laboratory bore-driven swash and cover a wide range of bed roughness. Data were obtained across the full width of the swash zone and are contrasted with data from the inner surf zone. Estimates of the flow velocities through the full swash cycle were obtained through numerical modelling and calibrated against measured velocity data. The measured stresses and calculated flow velocities were subsequently used to back-calculate instantaneous local skin friction coefficients using the quadratic drag law. The data show rapid temporal variation of the bed shear stress through the leading edge of the uprush, which is typically two-four times greater than the backwash shear stresses at corresponding flow velocity. The measurements indicate strong temporal variation in the skin friction coefficient, particularly in the backwash. The general behaviour of the skin friction coefficient with Reynolds number is consistent with classical theory for certain stages of the swash cycle. A spatial variation in skin friction coefficient is also identified, which is greatest across the surf swash boundary and likely related to variations in local turbulent intensities. Skin friction coefficients during the uprush are approximately

twice those in the backwash at corresponding Reynolds number and cross-shore location. It is suggested that this is a result of the no-slip condition at the tip leading to a continually developing leading edge and boundary layer, into which high velocity fluid and momentum are constantly injected from the flow behind and above the tip region. Finally, the measured stress data are used to determine the asymmetry and cross-shore variation in potential sediment transport predicted by three forms of sediment transport formulae.

---

* corresponding author. Fax: +63 7 3365499, mbarnes@uq.edu.au

Key words: Bed shear stress; Shear plate; Swash zone; Friction coefficient; Sediment transport; Beach morphodynamics; Boundary layer.

1. Introduction

Prediction of sediment transport in the swash zone remains a major challenge in coastal engineering. Despite recent advances in theoretical and numerical modelling (e.g. Kobayashi and Johnson, 2001; Pritchard and Hogg, 2005, Karambas, 2006; Calantoni et al., 2006; Baldock et al., 2008) and detailed field observations of sediment transport and beach morphology (Masselink et al., 2005; Weir et al., 2006; Aagaard and Hughes, 2006; Austin and Masselink, 2006; Hsu and Raubenheimer, 2006) models for beach profile evolution are poor and usually unable to correctly estimate net sediment transport directions and net deposition (see Masselink and Puleo (2006) and Brocchini and Baldock (2008) for recent reviews). This is despite the fact that relatively simple sediment transport models appear reasonably robust predictors of gross sediment transport rates in the swash zone (e.g. Masselink and Hughes, 1998; Butt et al., 2004).

While settling of pre-suspended sediment entering the swash has an important role to play in the net transport (e.g. Pritchard and Hogg, 2005; Alsina et al., 2005), the boundary shear stress is the fundamental and dominant driving mechanism for both bed load and suspended load (e.g. Nielsen, 1992). Bed shear stress is fundamental to improving swash sediment transport predictions, but present models tend to be based on approaches used for steady or oscillatory wave flows, neither of which are necessarily appropriate in the swash zone (e.g. Elfrink and Baldock, 2002; Masselink et al., 2005).

Measurements of bed shear stress in the swash are most often obtained indirectly from boundary layer velocity profile measurements. Controlled experimental investigations combined with advances in instrumentation and modelling ability have significantly furthered knowledge of boundary layer structure in steady and oscillatory flow regimes. In contrast, measurements of the boundary layer within swash remains a challenge, although Petti and Longo (2001), Cox et al (2000), Arcetti and Brocchini (2002), Cowen et al. (2003) and Raubenheimer et al. (2004) provide data close to the surf-swash boundary. However, significant difficulties with this approach arise at the leading and trailing edges of the swash, as a result of intermittent bubbly flow and very shallow flow depths. Conley and Griffin (2004) report hot-film measurements of swash bed shear stress in the field, a particularly challenging environment. Their data indicate friction coefficients over mobile sand beds an order of magnitude lower than other estimates from field data, so some uncertainty remains. In addition, the measurement location within the swash zone was not reported. As a result, a quantitative understanding of the cross-shore variation in swash zone bed shear stress is lacking.

The present paper addresses these issues by providing the first comprehensive data set of direct stress measurements obtained using a shear plate within the swash zone. The data are obtained from medium and large scale experimental facilities and include a wide range of different bed roughness. Swash zone friction coefficients are back-calculated using a combination of measured and modelled flow velocities. This paper is organised as follows. Section 2 provides a review of relevant theory and previous work. Section 3 outlines the experimental arrangement, instrumentation and flow conditions. Examples of the measured shear stresses are presented in Section 4, together with the modelling and analysis techniques applied to calculate friction coefficients. The detailed experimental results are presented in Section 5, and include the temporal variation of shear stress, Reynolds number and friction coefficient during individual swash flows, and the spatial variation of the maximum and minimum shear stresses and friction coefficients. The influence of bed roughness is also illustrated. Final conclusions follow in Section 6.

2. Previous work

Sediment transport modelling typically relies on bed shear stress estimated from the near bed logarithmic velocity profile. Close to the bed boundary, the fluid horizontal velocity U varies with height z above the bed according to the logarithmic velocity profile

$$U(z) = \frac{u*}{\kappa} \ln\left(\frac{z}{k_s}\right) + D_1 \qquad (1)$$

where u_* is the friction velocity, k_s is the bed roughness length, and κ is von Karman's constant (typically $\kappa = 0.40$). Schlichting (2000) defines the constant D_1 as 5.5 u_* for smooth turbulent flow and 8.5u_* for fully rough turbulent flow. Eq. (1) is commonly referred to as the law-of-the-wall or the log-law. The friction velocity u_* is related to the bed shear stress τ_0 through the relationship $\tau_0 = \rho\, u_*^2$ where ρ is the fluid density. However, the velocity profile is difficult to measure during swash, especially close to the fluid tip and towards the end of the backwash when depths are very small. This makes application of the log-law to determine swash bed shear stress problematic, except for highly controlled experimental conditions.

For uniform steady flow bed shear stress is related to the free-stream fluid velocity through a friction coefficient C_f (sometimes attributed to Fanning) via the quadratic relation

$$\tau_0 = \rho u_*^2 = C_f \frac{1}{2} \rho U^2 \qquad (2)$$

Equation (2) is widely applied for bed shear stress calculations under waves using a constant value friction coefficient. However, C_f is a function of Reynolds number and relative bed roughness, both of which vary substantially with time and space in the case of swash flow. Recent work by Nielsen and (2003) and Nielsen (2006) has modified the relationship between τ_0 and C_f, by accounting for temporal acceleration or allowing a time-varying friction coefficient. While a time-varying friction coefficient in the swash (using Eq. (2)) is well illustrated by Cowen et al. (2003), high shoreward temporal accelerations do not occur in swash, except close to the location of bore collapse (Hughes and Baldock, 2004; Baldock and Hughes, 2006; Puleo et al., 2007).

Swash friction coefficients have been inferred from bed shear stress estimates obtained from fitting the log-law to observed velocity profiles (e.g. Cox et al., 2000; Archetti & Brocchini, 2002; Cowen et al., 2003; Raubenheimer & Elgar, 2004; Hondebrink, 2006), or direct bed shear stress measurements (Conley & Griffin, 2004). The values of C_f obtained vary significantly ($0.001<C_f<0.054$). The variance is partly due to the method used to determine C_f, the experimental conditions, and the locations within the swash where measurements were made. A common finding is that C_f differs between uprush and backwash, with Cox et al. (2000), Archetti & Brocchini (2002), Cowen et al. (2003), and Conley and Griffin (2004) presenting time-averaged uprush coefficients C_{fu} that are typically greater than the time-averaged backwash coefficients $C_{fb.}$ Conversely, based on field measurements of swash velocity profiles, Raubenheimer et al. (2004) report no statistical difference between uprush and backwash friction coefficients. Some evidence suggests C_f may vary temporally and spatially over the swash cycle. However, only Cowen et al. (2003) and Hondebrink (2006) present detailed time-series of friction coefficients.

Despite providing a workable model, the law-of-the-wall may not actually be applicable at all times throughout the highly unsteady and non-uniform swash flow, especially at times of bore arrival, at flow reversal and towards the end of the backwash when flow depths are very shallow. Furthermore, inferring τ_0 from the log-law relies on precise knowledge of the elevation above the bed, z, where velocity measurements are taken. Accurately determining this in the field is difficult and a ±1cm error can lead to C_f being over- or under-predicted by 40% (Raubenheimer et al, 2004). Conley and Griffin (2004) attempted to address these issues via hot-film measurements. However,

1 their measurements yielded friction coefficients that are an order of magnitude lower
2 than friction coefficients obtained from other field data (e.g. Raubenheimer et al., 2004).
3 Co-located flow velocities were not measured by Conley and Griffin and the
4 measurement location within the swash zone was not reported; these add to the
5 uncertainties in the friction coefficients produced. Nevertheless, their result showing
6 higher friction coefficients in the uprush than in the backwash is consistent with some
7 previous results (e.g. Cox et al., 2000, Archetti & Brocchini, 2002, and Cowen et al.,
8 2003). An alternative to the log-law and hot film approaches is direct measurement of
9 the bed shear stress via the drag on a shear plate, which has been successfully applied
10 under wave motion (Grass et al., 1995; Myrhaug, 2001). Barnes and Baldock (2007)
11 reported the development of a shear plate designed specifically for deployment in the
12 swash zone and showed examples of direct stress measurements and friction
13 coefficients from smooth bed dam-break flows and swash flows. The shear plate
14 enables bed shear stress measurement from the moment of bore arrival to the very end
15 of the backwash. The fact that the plate measures bed shear stress at the very beginning
16 and end of the swash cycle is particularly important in the context of sediment transport
17 since the highest velocities and bed shear stresses occur at these times.
18
19 **3. Experimental setup**
20 Two series of laboratory experiments are presented:
21 1. Large scale solitary bore-driven swash experiments carried out using the
22 University of Aberdeen (UA) swash facility;
23 2. Medium scale solitary bore-driven swash experiments carried out in the
24 University of Queensland (UQ) wave flume.

In both cases a shear plate was used to make direct measurements of bed shear stress; corresponding measurements were made of the swash flow depths and velocities, as described in what follows.

2.1 The Swash Shear Plate

The design of the shear plate used to directly measure bed shear stress is based on the University College London (UCL) shear cell developed by Grass et al., (1995). Cross sectional diagrams of the shear cell are shown in Figure 1. Within the Perspex cell casing, four thin tubular sway legs support a removable smooth aluminium shear plate, 0.1m long, 0.25m wide and 0.73mm thick, with mass 94g. The four legs are clamped to the underside of the plate and extend to the base of the cell where they are fixed. The leg stiffness provides the restoring force and may be altered to suit the hydrodynamic forcing. Below the plate, two support rods fitted with stainless steel ball bearing rollers extend longitudinally, providing support against hydrostatic loading normal to the plate surface. The ball bearings provide 6 points of vertical support and rotate only fractionally following displacement of the plate above, resulting in minimal additional resistance over that provided by the tubular legs. This ensures a linear relationship between applied stress and plate displacement. Different roughness elements may be glued to the plate as required.

The applied shear forces cause the plate to be displaced in the plane of the plate, or tangential with the shear. To allow for the displacement, a 1mm gap exists between the plate edges and the Perspex cell casing. The plate position may be adjusted within the cell to remove static displacements, e.g. when mounted on a slope. During operation the shear cell is filled with water, including the 1mm gap at the plate edges. Surface

tension is sufficient to hold the water in the gaps even when mounted on bed slopes up to 1:10. The horizontal displacement of the shear plate is measured by a single Indikon Eddy-current Proximity Probe, aligned perpendicular to a target plate attached on the underside of the shear plate. The Eddy-current probe senses displacements with a resolution of order 0.001mm. The plate is capable of measuring bed shear stress in both flow directions and does not require any assumptions to be made about the flow structure. The plate may be mounted horizontally or on a sloping beach without changing the measurement principles.

As documented by Riedel (1972), Riedel & Kamphuis (1973), Grass et al. (1995), and Rankin & Hires (2000), the displacement of a shear plate under oscillatory waves is not solely due to the shear stress acting on the surface of the plate. Oscillatory flow conditions require or generate pressure gradients leading to inertial (Froude-Krylov) forces that are proportional to the plate volume. For the present experiments small pressure gradients across the plate are caused by the slope of the free-surface η across the plate x, as illustrated by Figure 2. The pressure gradient across the shear plate, dp/dx, was measured via pressure tappings located slightly below the plate (refer Figure 1) and two Druck PMP 317-2780 pressure transducers with ±0.15% accuracy (GE Druck, 2006). The bed shear stress τ_0 was then obtained from the total force F_T measured by the plate and the measured pressure gradient dp/dx according to:

$$\tau_0 = \frac{F_T - F_{PG}}{A_{plate}} = \frac{F_T + \frac{dp}{dx} V_{plate}}{A_{plate}} \qquad (3)$$

where A_{plate} and V_{plate} refer to the plate surface area and plate volume respectively, and dp/dx is positive for a seaward-dipping water surface. For the bed stresses reported here,

the pressure gradient contributions to the measured force are usually small and an example of the measured total force F_T, pressure gradient force F_{PG}, and resulting bed shear stress τ_0 is provided in Section 3 (Figure 5). Since the water surface dips seaward for the majority of the swash flow (Baldock and Hughes, 2006), the pressure gradient acts against the shear stress during uprush, and acts with the shear stress during backwash. Simultaneous measurements of the flow depth above the plate with ultrasonic displacement sensors match the pressures measured below the plate nearly identically, indicating hydrostatic conditions within the gaps. In addition, dye injected into the cell shows minimal currents are generated on the underside of the plate, and therefore any shear force on the underside of the plate is negligible and ignored.

Calibration of the shear plate force/displacement relationship was performed in-situ for each deployment, using a pulley and weight system. A known mass was used to displace the shear plate tangentially (simulating hydrodynamic forcing) and the Eddy sensor output recorded. This was repeated for different weights, giving a linear calibration curve for displacements up to the maximum possible. Point static load tests at different locations over the plate showed that the plate does not respond to differential normal pressure forces, verifying that the supporting roller system works as intended. Consequently, no additional tangential displacement of the plate is expected to occur when the variable-depth leading edge of the swash front propagates across the plate.

2.2 The University of Aberdeen Experiments

Large-scale experiments investigating bore-driven swash were conducted at the UA Fluid Mechanics Laboratory. The swash facility, Figure 3, is built into an existing 20 m long, 0.45 m wide and 0.9 m deep flume. A reservoir of water is held by a gate at

one end of the flume. In front of the gate is water with depth equal to 0.1 times the water depth in the reservoir. A high speed vertical removal of the gate releases the reservoir of water into the shallow quiescent water. This mechanism produces a single plunging breaker that evolves to form a bore that propagates approximately 4.0 m before collapsing at the still water line (SWL) and initiating a highly repeatable swash event (Hondebrink, 2006). Experiments were conducted on an impermeable smooth Perspex beach and on an impermeable rough beach constructed by gluing pebbles 5 - 6 mm in size onto the Perspex beach panels. All of the UA experiments involved a beach slope of 1:10 and a reservoir depth of 0.65 m.

Direct shear stress measurements were obtained with the swash shear plate installed at two cross-shore locations, $x = 2$ and $x = 3$ m, where x is measured relative to the SWL, positive shoreward. Maximum swash run-up was measured along the slope and equal to $R_x = 5.7$m and $R_x = 4.6$m for the smooth and rough beaches respectively. Surface elevation η and flow depth h were measured using a roving array of Microsonic© acoustic displacement sensors, model Mic+25/IU/TC (MS25). Fluid velocity measurements for the same test conditions were available from a previous study (Hondebrink, 2006) in which detailed velocities were measured at various cross shore locations using particle image velocimetry (PIV). The measurements yielded the time-dependent velocity profiles and the depth-averaged velocity time-series, ensemble-averaged over 50 repeats of the swash event. The Hondebrink measurements resolve the flow to a high level of detail, both temporally and spatially. However, the measurements do not capture velocities at the time of bore arrival (because of air entrainment in the bore) and towards the very end of the backwash (because of the very

shallow depths).. This is also true for the LDA measurements by Cox (2000) and the PIV data of Cowen et al. (2003).

2.3 The University of Queensland Experiments

Solitary wave experiments were conducted at the UQ Gordon McKay Hydraulics Laboratory. The UQ solitary wave flume is 20m long, 0.85 m wide, 0.75 m high (figure 4). The flume has an impermeable bed, glass walls and a 1:12 slope beach constructed from marine plywood. Beach roughness is varied by fixing different materials to the beach surface. In the present investigation measurements were obtained for an impermeable smooth marine plywood beach and an impermeable coarse sandpaper (d_{50} = 0.2mm). A single bore is generated by a piston wave maker with bore height H controlled by the piston stroke length L and speed V, with a bore propagation distance of approximately 8 m in quiescent water before the shoreline is reached. Provided the piston stroke is of sufficient speed, the bore generates at the wave maker and is fully developed upon reaching the shoreline for the range of water depths used in this study ($0.15<h<0.22$m). These conditions generate medium scale swash events ($2.3<R_x<2.8$m) and measurements of swash depths compare well with recent theory (Guard and Baldock, 2007; Pritchard et al., *in press*).

The beach was constructed in a series of removable panels of identical dimensions. The swash shear plate was installed within one such panel and substituting that panel with neighbouring panels allowed direct shear stress measurements to be obtained at five cross-shore locations. Furthermore, variation of the initial depth, h, in the flume also changed the shear plate location relative to the SWL, providing data at more cross-shore locations, x/R_x. Surface elevation, η, and flow depth, h, were measured

using an array of roving MS25 sensors, and at the edges of the shear plate. Maximum swash run-up, R_x, was measured manually by marking the maximum landward extent of the uprush and measuring back from the mark to the SWL. Instantaneous free-stream velocity components were measured using a 2D side-looking Acoustic Doppler Velocimeter (ADV) at locations seaward of the SWL, again to validate the NLSW flow model. A single Microsonic Mic+35/IU/TC (MS35) sensor was aligned above the ADV sample volume to measure bore height H and water surface elevation. Surface elevation and fluid velocity were also measured at a single offshore location to provide seaward boundary conditions for the numerical modelling. Table 1 summarises the UA and UQ experimental conditions.

3. MEASUREMENTS & MODELLING

The typical temporal variation in measured shear stress, τ_0, swash surface elevation, η, total force, F_T, and the pressure gradient force, F_{PG}, is presented in Figure 5. The local swash event commences when the uprush fluid tip arrives at the measurement location, and defined as the instant when the measured depth at the tip exceeds 3mm. The local swash period, T, is defined as the total time of the swash event at the measurement location, and is used later to normalise the absolute time-scales. The definition of the local swash event follows that suggested by Hughes and Moseley (2007). The surface elevation gradient across the plate $d\eta/dx$ is obtained from the pressure transducer measurements and ultrasonic transducers at the landward and seaward plate edges. Figure 5 shows a predominantly seaward directed pressure gradient throughout the swash cycle. With regard to the total force, F_T, measured by the plate, the pressure force, F_{PG}, is insignificant for the majority of the uprush but can become significant in the backwash as a relatively strong favourable pressure gradient

develops as the water surface slope approaches the beach slope. Note that F_{PG} is plotted on the secondary axis and is an order of magnitude smaller than the primary axis. The bed shear stress time series shows a maximum positive (landward directed) stress at the time of arrival of the bore, followed by a rapid decay in the shear stress throughout the remainder of the decelerating uprush. Following flow reversal, the maximum negative (seaward directed) shear stress occurs late in the backwash phase, with the stress reducing toward zero at the end of the backwash.

An example of the typical temporal variation of swash flow depth, h, bed-parallel velocity, U_x, and bed shear stress are presented in Figure 6. Note that conditions close to the wet/dry interface, and the associated shallow flow depths, challenge the PIV technique and therefore velocity measurements are not available at the swash leading edge and late in the backwash. Consequently, numerical modelling was performed to obtain estimates of the horizontal swash velocities at these phases of the flow. Modelled velocities associated with flow depths < 4mm were discarded. These calculated flow velocities have sufficient resolution to enable estimates of swash friction coefficients to be derived from the measured stresses at the fluid tip and at the end of the backwash. The experimental conditions were simulated using the ANUGA hydrodynamic model (Nielsen et al., 2005), which solves the non-linear shallow water equations using a finite volume method, with particular attention to resolving the dry/wet boundary, and including friction. ANUGA has been extensively tested under a wide range of flows (e.g. Nielsen et al., 2005; Rigby & Van Drie, 2008), including swash flows and dam-break flows (Baldock et al., 2007; 2008). Here, predicted depth-averaged velocities from the model are used to provide representative free-stream velocities when back-calculating friction coefficients using Eq. (2). Note that ANUGA uses a constant

Manning's friction coefficient, *n,* to simulate be friction in the momentum equation, so the chosen *n* (obtained through root mean square error analysis comparing measured and predicted flow depth and runup) and resulting back calculated friction coefficients are unrelated.

For the UA swash experiments, the measured depths and the velocities measurements of Hondebrink (2006) at x = 2m and x = 3m were used for model verification. The UA smooth beach results are presented in Figure 6. Measured and predicted swash depths are in good agreement for the entire swash event and predicted flow velocities are in good agreement with the data for periods when reliable data are available. For the UQ wave flume experiments, the offshore water surface elevation and horizontal velocity were measured and used as input at the model seaward boundary at x = -4.6m. Modelled and measured flow depths are compared in figure 7, and again the agreement is good.

ANUGA is a finite-volume depth-averaged Non-Linear Shallow Water Equation (NSWE) solver. Vertical velocities and the vertical structure of the flow are not resolved by the model. Despite this, predicted hydrodynamics compare well against measured offshore (inner surf zone) bore characteristics (Figure 8) where significant turbulence associated with the fully developed bore is present. However, the maximum shoreward velocity under the bore front tends to be overestimated, possibly due to the comparison of a point measurement to a depth-averaged prediction, or because the ADV measurement is low due to signal contamination caused by the aerated flow condition. If the model over predicts the initial shoreward velocities in the swash, then it should be noted that the estimates for C_f will be underestimated. Nevertheless, the phase of the

velocity is well predicted. A notable breakdown in the model is related to the 'bore collapse' at the SWL. As discussed by Yeh et al. (1989), according to shallow-water wave theory the bore height vanishes at the shoreline and a rapid and total conversion of potential to kinetic energy occurs. Vertical accelerations are therefore likely to be important during bore collapse, and as a result the observed transition from bore to swash is not modelled exactly by NSWE solvers, particularly the exact time-scale over which bore collapse occurs. Consequently, a single small negative correctional shift to the model time base was necessary following bore collapse to correctly match the measured and modelled arrival time of the swash tip (e.g. figures 6 and 7). This then ensures the correct phase relationship between measured and modelled velocities and surface elevation. This is demonstrated by the close match between modelled and measured times of flow reversal shown in figure 6.

4. RESULTS

4.1 Temporal variation in shear stress and friction coefficient

Figure 9a illustrates the temporal variation of the bed shear stress and back-calculated friction coefficient for the UA experiments with smooth Perspex bed. C_f based on the measured and predicted velocities are included. The instantaneous Reynolds number, Re,

$$\mathrm{Re} = \frac{\rho D_h U_x}{\mu} \qquad (4)$$

is also plotted, where μ is the fluid dynamic viscosity and the hydraulic diameter D_h is defined as the ratio of four times the cross-sectional area and the wetted perimeter P_w

$$D_h = \frac{4A}{P_w} \qquad (5)$$

The shear plate provides data with very little noise, although it should be noted that the measured stress represents a spatial average over the plate area. However, the plate length is only a small fraction (2%-3%) of the total run-up length and therefore resolves the stress from a relatively narrow zone of the swash zone. The shear stress is largest at the time of bore arrival and reduces rapidly during the uprush. The shear stress remains small for an extended part of the backwash, and the maximum offshore directed stress is less than half the peak onshore stress. The data clearly demonstrate that the bed shear stress does not lead the free stream velocity, consistent with a decelerating uprush (Baldock and Hughes, 2006), which is qualitatively different behaviour from that observed in wave boundary layers (e.g. Nielsen, 1992). Indeed, during the initial backwash, the shear stress appears to lag the flow velocity. The instantaneous Reynolds number varies rapidly through the swash cycle, reaching a peak of order 10^5 during the uprush, which is well into the turbulent flow regime. The maximum Reynolds number in the backwash is typically half of that in the uprush. During the initial uprush phase and late in the backwash friction coefficients based on measured velocities differ from friction coefficients based on predicted velocities. Friction coefficients obtained via Eq. 2 are sensitive to the value of U_x and at the swash leading edge and late in the backwash the PIV measured velocities are significantly smaller (leading to higher C_f) than the predicted velocities (refer Fig. 6). Behind the leading edge measured and modelled velocities are consistent and the friction coefficient remains quite constant over the remaining uprush flow. The friction coefficient is poorly defined during the period of flow reversal, but is very small for an extended part of the backwash. This is a common feature of all the measurements, and is considered further below.

Figure 9b shows the corresponding results for the UA experiments with the rough bed. The bed shear stress at the time of bore arrival shows significantly different behaviour for this case, with a very large shear stress at the swash tip, which drops very rapidly as the front passes the shear plate. Some discrepancy between C_f based on measured velocities and C_f based on modelled velocities is again observed at the early and late stages of the swash cycle. The maximum friction coefficient is associated with the arrival of the fluid uprush tip ($t/T \approx 0$), followed by a decay in C_f with increasing Re. The minimum uprush C_f occurs at the maximum Re. As the backwash phase commences C_f rapidly decreases with increasing Re, reaches a minimum value at the maximum backwash Re, and steadily increases as Re decreases thereafter (C_f tends to infinity as U_x and Re tends to zero). Figure 9b provides evidence of the instantaneous swash friction coefficient C_f decreasing with increasing instantaneous Re. This general behaviour in C_f is consistent with that known for steady and oscillatory flow regimes.

For these rough bed results, the magnitude of the peak stress and friction coefficient increased by nearly an order of magnitude compared to the smooth bed case. If it is assumed that the Perspex bed corresponds to nearly hydraulically smooth flow conditions, while the rough bed corresponds to fully rough flow conditions, then this increase in peak C_f is significantly greater than that expected for steady flows with a similar difference in roughness. Similarly, the magnitude of peak C_f, or equivalently, τ_0, is significantly larger than that expected for equivalent steady flows. The maximum backwash shear stress is less than one-third of the peak uprush stress, but is of longer duration.

The dash-line in Figure 9a and 9b (also in Figure 10a and 10b) is a time-varying friction coefficient based on the Colebrook-White formula for turbulent, steady, uniform open channel flow (Colebrook, 1939)

$$\frac{1}{\sqrt{f}} = -2\log_{10}\left(\frac{k_s}{3.71D_h} + \frac{2.51}{\mathrm{Re}\sqrt{f}}\right) \quad (6)$$

Where f is Darcy-Weisbach friction factor (related to the Fanning friction factor, C_f, through $f = 4C_f$), D_h and Re are local, instantaneous values and the equivalent roughness k_s is simply obtained following

$$k_s \approx 2.5d_{50} \quad (7)$$

Figures 10a and 10b present similar results from the UQ swash experiments with fixed sandpaper bed (d_{50}=0.2mm); results are shown for both the lower (x/R_x=0.25) and the upper swash zone (x/R_x=0.83) measurement locations. A similar pattern to the UA results is seen in the shear stress and C_f behaviour, although the decrease in C_f after the swash tip passes the measurement location is less marked than for the UA rough bed experiment. Significant offshore stresses again only develop late in the backwash.

The Colebrook-White time-varying C_f typically under-predicts the uprush back-calculated C_f and over-predicts the backwash back-calculated C_f. Under-prediction in the uprush may be due to the presence of bore-related turbulence. Over-prediction in the early backwash is potentially due to a transitioning flow regime where the application of the Colebrook-White formula is invalid.

4.2. Spatial variation in shear stress and friction coefficient

Figure 11a shows the cross-shore spatial variation in the peak uprush (positive) and backwash (negative) bed shear stresses from the UQ experiments. The results are

shown for the two beach materials (smooth marine plywood and sandpaper). The ensemble-averaged uprush and backwash maximum bed shear stresses (typically average of five repeat swash events), at each cross-shore location, are normalised by the maximum measured uprush bed shear stress, $\tau_{0uprush\ max}$. Error bars indicate the standard deviation of the measurements. The maximum shear stress increases significantly between the inner surf zone just prior to bore collapse ($x/R_x \approx$-0.05) and the lower swash zone ($x/R_x \approx$0.05-0.2), with an approximately five-fold increase in the peak uprush shear stress. The maximum uprush bed shear stress across the swash zone is typically 3-4 times greater than the maximum backwash bed shear stress. However, for the inner surf zone ($x/R_x < 0$) the seaward directed maximum stress is approximately 1.5 times greater than the landward directed maximum stress. A gradual reduction in peak bed shear stress was observed for $x/R_x > 0.3$.

Figure 11b shows the friction coefficients corresponding to the maximum bed shear stresses presented in Figure 11a. C_{fmax} is obtained from Eq. (2) using the ensemble-averaged measured peak bed shear stress, τ_{0max}, and the maximum depth-averaged horizontal velocity U_x predicted by the ANUGA model. For swash zone locations, and a given bed roughness, C_{fmax} during the uprush is typically twice C_{fmax} during the backwash. The uprush friction coefficient associated with the maximum stress shows more spatial variation than the equivalent backwash friction coefficient, most likely caused by the turbulent structure of the swash uprush leading edge. Mean C_f for the sandpaper bed is approximately 1.7 times the smooth plywood bed mean C_f. This increase again appears greater than that expected for steady flows with a similar change in bed roughness.

4.3. Variation with local Reynolds number

The variation of instantaneous friction coefficient with local Reynolds number for the UA pebble beach experiment is presented in Figure 12a for uprush and Figure 12b for backwash. Only friction coefficients based on model-predicted velocities are included. The large C_f associated with small Re calculated at times near flow reversal (C_f trends toward infinity as U_x and Re trend toward zero) are not plotted. The start of each data set in time (for uprush the arrival of the fluid tip, for backwash the first value plotted following flow reversal) is indicated by the bold symbol.

The uprush results (Figure 12a) show a typically decreasing C_f with increasing Re, again consistent with the general behaviour of friction coefficient for steady and oscillatory flows. Figure 12a suggests for a given cross-shore location local Re may provide a practical description for C_f, however the same local Re yields a significantly different C_f when different cross-shore locations are considered.

The backwash results (figure 12b) suggest local Re poorly describes C_f. Following flow reversal, C_f rapidly decreases before reaching a minimum that is closely associated with the local maximum Re. The maximum Re remains constant for a short period while C_f increases. During this period the increasing backwash fluid velocity and decreasing flow depth balance in the calculation of Re. However, the increasing bed shear stress leads to an increase in C_f (refer Figures 9a&b). For the remainder of the backwash phase a decreasing Re is coupled with an increasing C_f.

The sensitivity of C_f and Re in terms of cross-shore location is due to the variation in fluid velocity, U_x, and flow depth, h. For periods where the variation in U_x

and h balance in the calculation of Re (as shown in Figure 12b for the UA pebble beach backwash) a variation in C_f may be observed, since its definition is independent of h. In field swash, for a given cross-shore location, constant Re may be encountered for a short period during the uprush (Re invariant due to an increasing h and decreasing U_x) or during the backwash (Re invariant due to a decreasing h and increasing U_x) depending on the swash conditions largely dictated by the incoming bore characteristics and beach gradient. The potential for invariant Re while the velocity changes indicates that the local flow Re is generally likely to be an inadequate descriptor of swash C_f at certain times during the swash flow.

5. Discussion

The results show that maximum shear stress at the leading edge of the swash is usually 2-4 times greater than maximum bed shear stress in the backwash, with correspondingly larger skin friction coefficients in the uprush compared to the backwash. These data are consistent with data from Cox et al. (2000), Cowen et al. (2003) and Conley and Griffin (2003) who obtained results from a single location in the swash zone and a single bed roughness. However, the present data show that this difference in C_f is maintained across the full width of the swash zone, and indeed the asymmetry between the maximum uprush and maximum backwash stress tends to increase landward. In addition, for a range of bed roughness, the results show that the skin friction in the uprush is typically larger than that expected for equivalent steady flows, while the skin friction in the backwash appears lower than expected. The former condition is consistent with a developing swash leading edge, where fluid from behind the leading edge overruns the fluid right at the swash tip, since there is a no no-slip condition at the boundary. Hence, high velocity fluid and momentum are constantly

injected at the leading edge from the flow above and behind the tip. Behind the tip region in the main body of the flow, the boundary layer growth during the decelerating uprush and the accelerating backwash is expected to be different (Elfrink and Baldock, 2002) and boundary layer growth and behaviour depends on the flow history from the time of initial motion, or the preceding flow reversal (e.g. Nielsen, 2002; Masselink et al, 2005). Local shoreward directed flow acceleration within the swash has been regarded as important in this respect (Nielsen, 2002; Puleo et al., 2003). However, Hughes and Baldock (2004), Baldock and Hughes (2006) and Puleo et al. (2007) show that any such shoreward directed accelerations are limited to the zone of bore collapse at the seaward swash boundary. Indeed, it is the backwash flow that is accelerating, but the shear stress appears lower than expected during that phase of the flow. Nevertheless, the flow history during uprush and backwash is quite different (Hughes et al., 1997; Masselink and Hughes, 1998), which, together with different turbulence levels (Petti and Longo, 2001; Hughes et al., 2007), is expected to lead to different boundary layer growth and the asymmetry in the bed stress.

This flow history is illustrated in figure 13, which plots numerical model predicted fluid particle trajectories through the uprush and backwash for conditions corresponding to the UA smooth Perspex beach experiment. The trajectories are calculated by post-processing the flow field obtained from the ANUGA model, using the Eulerian-Lagrangian transformation proposed by Alsina et al. (2005) and Pritchard and Hogg (2005). Although these trajectories are obtained from a 1-D numerical model, this approach has been found to compare well with experimental measurements of fluid particle advection across the surf-swash zone boundary (Baldock et al., 2008). The fluid trajectories show that all the flow acceleration (convergence of trajectory lines)

during the uprush occurs seaward of the SWL, which is combined with turbulence from the bore injected toward the bed boundary layer (Cowen et al., 2003; Butt et al., 2004), and both effects may be expected to result in a thin boundary layer as the initial condition at the start of the uprush. In this inner surf zone region, the wave boundary layer model of Nielsen and Callaghan (2003), which includes the influence of fluid acceleration, may be appropriate. In combination, the fluid trajectories and the rapid increase in C_f at the SWL (figure 9b) suggest that these influences on the wave boundary layer occur in a very narrow region just before the shoreline. In addition, boundary layer growth will have commenced progressively further offshore for particles entering the swash later in the uprush. Shoreward of the SWL the uprush flow is diverging and the boundary layer is subject to a weak adverse pressure gradient. The boundary layer development during this phase of the flow may then be more consistent with the development of the boundary layer that forms as a flow encounters a flat plate than an oscillatory wave boundary layer, i.e. a thin boundary layer exists at the start of the swash zone, which then grows as the flow progresses (Cowen et al., 2003; Masselink et al., 2005). Since the boundary layer is growing, rather than steady, at any instant it must be thinner than that expected for an equivalent steady flow at the same relative roughness and Reynolds number. This is consistent with the higher values for C_f observed during the uprush. An unsteady flow flat plate model for the swash boundary layer will be considered in a later paper. However, it appears that it will be necessary to account for the flow history, possibly by determining the boundary layer thickness in terms of the integrated products of the velocity and particle displacement.

The relatively slow increase in bed shear stress with time during backwash is significant in terms of the potential sediment transport carried by the backwash, which

has been observed to be smaller than the uprush transport (e.g. Masselink and Hughes, 1998). While this late development of the shear stress does not appear to have previously been reported for the swash zone, it appears consistent with turbulence measurements presented by Aagaard and Hughes (2006), who observed that significant turbulence in the vertical flow component appears only late in the backwash. Similarly, Cowen et al. (2003) report backwash turbulence levels that are lower than expected from steady flow flat plate boundary layer theory. A number of possible explanations appear consistent with these results. Firstly, the increasingly favourable pressure gradient that exists after flow reversal, which may keep the backwash boundary layer laminar for a longer period than expected. Secondly, the Reynolds number also increases more slowly in the backwash, and only reaches values of order 10^5 quite late in the flow. This Reynolds number corresponds to the range expected for transition from a laminar boundary layer to a turbulent boundary layer flow for smooth flat plate conditions. In a Lagrangian reference frame, following the particle trajectories (figure 13), the effect of the flow history after flow reversal suggests, that at any instant, the boundary layer will be closer to a laminar flow regime than if the flow prior to that time had been a steady flow at the same velocity. Hence, the viscous sub-layer may be thicker than for an equivalent steady flow, which would have the effect of reducing the effective bed roughness. Finally, the flow is accelerating in the backwash. Hence, the skin friction resistance must be lower than for an equivalent steady flow with the same Reynolds number and relative roughness.

Despite the temporal variation of C_f, some success can be gained from application of Equation 2, but a different C_f for uprush and backwash. This is because of the dominance of the U^2 term in determining the bed stress. Figure 14 shows measured

and predicted τ_0 in the lower-mid swash zone for the UQ swash experiment. The uprush and backwash C_f have been selected to best-fit the measured peak (maximum) uprush and backwash shear stress: uprush C_f=0.015 and backwash C_f=0.009. By matching the maximum stresses, a reasonable comparison throughout the swash cycle appears possible, although the predicted shear stress is then overestimated for the initial part of the uprush and backwash. While previous experiments have determined mean friction coefficients for the swash zone (e.g. Cowen et al., 2003; Raubenheimer et al., 2004; Conley and Griffin, 2003), the data have been obtained at only a single cross-shore position or the location was unreported. $<C_f>$ for uprush and backwash, where $<>$ denotes time-averaging over the uprush or backwash phase, obtained at different cross-shore locations during the UQ and UA experiments are shown in figure 15. The data show no clear dependency on cross-shore location within the swash zone. Therefore, despite previous observations (e.g. Cowen et al, 2003) and the present data suggesting that applying a constant C_f through the uprush and backwash phases of the swash cycle is physically unjustified, adopting a temporally and spatially constant value of C_f for estimates of gross sediment transport rates in one direction remains a potentially useful Engineering approach. The most common application where such an approach appears justified is swash overtopping (e.g. Kobayashi and Tega, 1996; Baldock et al., 2005).

Finally, the ability of the shear plate to measure at the leading edge of the uprush and late in the backwash enables a good estimate of the likely asymmetry in potential sediment transport during these swash events. Three forms of transport model are tested; $q = \tau_0 U$; $q = \tau_0 U^2$; and $q = \tau_0 U^2 h$, which correspond to a Shields type transport model, a Bailard (1981) type suspended load transport model and a suspended load transport model where the sediment flux depends on the local depth (e.g. Pritchard and

Hogg, 2005), respectively. The spatial variation of the following terms: $<|\tau_0|U>, <\tau_0 U^2>, <\tau_0 U^2 h>$, were calculated from the measured stress data and the predicted flow velocities, and where <> denotes time-averaging over the swash event and τ_0 is the measured stress. It should be noted that these estimates assume some similarity between the asymmetry in the bed shear stress between fixed, impermeable and mobile, permeable sediment beds. While it is recognised that the friction coefficients will be higher for mobile beds as a result of increased roughness, no data yet exists regarding the cross-shore variation of time-varying friction coefficients for mobile beds in the swash zone. Consequently, the results presented in figures 16a – 16c do not directly apply to mobile, permeable beds, but perhaps provide an indication of the influence of shear stress asymmetry. Figure 16a shows that $<|\tau_0|U>$ is predominantly directed offshore through the lower swash zone, but there is little asymmetry or a landward directed trend of this parameter higher on the beach face. The potential suspended load transport according to a Bailard-type model ($<\tau_0 U^2>$) is offshore seaward of the SWL and onshore throughout the swash zone, but is relatively low above the mid-swash zone (figure 16b). Note that this form of model corresponds to suspended load transport entrained within the swash zone and the rapid reduction in transport potential above the mid-swash zone is due to the transport being a function of high powers of *U*. If the suspended sediment flux is a strong function of the flow depth, i.e. assuming a uniform sediment concentration over the depth, then the predicted suspended load transport also remains onshore throughout the swash zone (figure 16c), but is again only weakly onshore above the mid-swash zone. For mobile beds pre-suspended sediment is advected into the swash from the inner surf zone, and usually settles during the uprush. This transport is in addition to the predicted transport presented in figures 16b and 16c.

5. Conclusions

The first comprehensive data set of direct bed shear stress measurements obtained from a shear plate in the swash zone has been presented. The data were obtained from medium and large scale experimental facilities and include a wide range of bed roughness. A combination of the directly measured data and numerical modelling enabled estimates of skin friction coefficients throughout the swash cycle, including the leading edge of the uprush. The results demonstrate that the maximum bed shear stress occurs at the leading edge of the shoreline and that the maximum uprush bed shear stress is typically 2-4 times greater than the maximum backwash bed shear stress. The maximum shear stress in the uprush and backwash are higher and lower than that for equivalent steady flow, respectively. It is suggested that the high shear stress at the leading edge is a result of the no-slip condition at the tip, leading to a continually developing leading edge and boundary layer, into which high velocity fluid and momentum are constantly injected from the flow behind and above the tip region. The backwash flow history differs from that during the uprush, and the backwash shear stress appears to lag the free stream velocity, with significant bed shear developing only late in the backwash.

Temporal variation of the skin friction coefficient, C_f, occurs throughout the entire swash cycle. C_f is observed to typically decrease with increasing Reynolds number and vice-versa. The temporal variation of C_f is greatest in the backwash, but is also significant for rough beds during the uprush. During uprush, the friction coefficient associated with the peak stress varies spatially across the beach face, with a rapid increase at the surf-swash boundary and a gradual decrease further shoreward. The spatial variation of C_f is less marked in the backwash. Taking a temporal average over

each phase of the swash cycle, the skin friction coefficient during the uprush is approximately twice that during the backwash. However, despite evidence of temporal and spatial variation in C_f, applying the quadratic drag law with a constant friction coefficient remains a useful engineering approach for calculating gross sediment transport rates, for example during swash overwash.

Finally, measured stresses were used to estimate the cross-shore variation and assymmetry in sediment transport formula. For a single swash event considered here, a Shields-type transport model predicts net offshore transport in the lower swash and a Bailard-type model predicts shoreward transport across the whole swash zone. In the inner surf zone, the models predict net offshore transport. However, sediment transport in the inner surf zone and lower swash zone are strongly dependent on additional processes not considered by simple transport models including sediment pickup, advection and deposition. Consequently, Eulerian estimates of bed shear stress or transport rates are unlikely to be robust indicators of net sediment transport gradients and morphological change.

Acknowledgements

The authors thank Paul Guard for assistance with experiments and gratefully acknowledge support from the UQ Graduate School and Sustainable Tourism CRC in the form of research scholarships for MB. The review comments of Prof Gerd Masselink and Dr Michael Hughes are appreciated and helped improve the manuscript.

References

Aagaard, T., Hughes, M.G., Møller-Sørensen, R., Andersen, S., 2006. Hydrodynamics and sediment fluxes across an onshore migrating intertidal bar. J. Coast. Res., 22, pp. 247-259 Scopus.

Alsina, J.M., Baldock, T.E., Hughes, M.G. Weir, F., Sierra, J.P., 2005. Sediment Transport Numerical Modelling in the Swash Zone. Coastal Dynamics. CD-ROM.

Archetti, R., Brocchini, M., 2002. An integral swash zone model with friction: an experimental and numerical investigation, Coastal Eng. 45, pp. 89–110 Scopus.

Austin, M.J., Masselink, G., 2006. Observations of morphological change and sediment transport on a steep gravel beach. Mar. Geology, 229, pp. 59 – 77 Scopus.

Bailard, J.A., 1981. An energetics total load sediment transport model for a plane sloping beach. J. Geophys. Res., 86 C2, pp. 10938–10954 Scopus.

Baldock, T.E., Hughes, M.G., 2006. Field observations of instantaneous water slopes and horizontal pressure gradients in the swash. Cont. Shelf Res., 26, pp. 574-588 Scopus.

Baldock, T.E., Hughes, M.G., Day, K., Louys, J., 2005. Swash overtopping and sediment overwash on a truncated beach, Coastal Eng., 52, pp. 633–645 Scopus.

Baldock T.E., Barnes, M.P., Morrison, N., Shimamoto, T., Grey, D., Nielsen, O., 2007. Application and testing of the ANUGA tsunami model for overtopping and coastal sediment transport, Proc. Coasts and Ports, CD-ROM.

Baldock T.E, Kudo, A., Guard, P.A., Alsina, J.M., Barnes, M.P., 2008. Lagrangian measurements and modelling of fluid advection in the inner surf and swash zones. Coastal Engineering., *55, 791-799* Scopus.

Barnes, M. P., Baldock, T. E., 2007. Direct bed shear stress measurements in laboratory swash, Journal of Coastal Research, SI 50, 641-645.

Brocchini, M., Baldock, T. E., 2008. Recent advances in modelling swash zone dynamics: Influence of surf-swash interaction on nearshore hydrodynamics and morphodynamics, Reviews of Geophysics, 46, RG3003, 1-21.

Butt, T., Russell, P., Puleo, J.A., Miles, J., Masselink, G., 2004. The influence of bore turbulence on sediment transport in the swash and inner surf zones. Cont. Shelf Res., 24, pp. 757–771 Scopus.

Calantoni, J.C., Puleo, J.A., 2006. Simulation of sediment motions using a discrete particle model in the inner surf and swash zones, Cont. Shelf Res., 26, pp. 610-621 Scopus.

Colebrook, C. F., (1939). Turbulent flow in pipes, with particular reference to the transition region between smooth and rough pipe laws. J. Ist. Civil Engrs., Feb. 1939.

Conley, D. C., Griffin, J. G., 2004. Direct measurements of bed stress under swash in the field. J. Geophys. Res. (Oceans), 109, C03050 Scopus.

Cowen, E.A., Sou, I.M., Liu, P.L.F., 2003. Particle image velocimetry measurements within a laboratory-generated swash zone. J. Eng. Mech., 129, 10, pp. 1119–1129 Scopus

Cox et al., 2000 Cox, D.T., Hobensack, W.A., Sukumaran, A., 2000. Bottom stress in the inner surf and swash zone. Proceedings 27th International Conference on Coastal Engineering, ASCE, pp. 108–119.

Dean, R.B., 1978. Reynolds number dependence of skin friction and other bulk flow variables in two-dimensional rectangular duct flow, Trans. ASME J. Fluids Eng., 100, pp. 215–223.

Elfrink, B., Baldock, T.E., 2002. Hydrodynamics and sediment transport in the swash zone: a review and perspectives. Coastal Eng. J., 45, pp. 149–167 Scopus

Fredsoe J (1984) Turbulent boundary layer in wave current motion. American Society of Civil Engineers Hydraulics Division 110 (HY8):1103–1120 Scopus

GE Druck, 2006. Automotive Pressure Transducers – PMP 317, website: http://www.gesensing.com/products/pmp_317.htm?bc=bc_ps+bc_drucks.

Grass, A. J., Simons, R. R., Maciver, R. D., Mansour-Tehrani, M., Kalopedis, A., 1995. Shear cell for direct measurement of fluctuating bed shear stress vector in combined wave/current flow. Proc. XXVIth IAHR Congress: HYDRA 2000, 1, pp. 415-420.

Guard, P.A., Baldock, T.E., 2007. The influence of seaward boundary conditions on swash zone hydrodynamics, Coastal Eng., 54, pp. 321–331 Scopus

Hondebrink, L.J., 2006. Numerical and Experimental Study of Bore-Driven Swash on Impermeable Slopes. PhD thesis, University of Aberdeen, 192 pp.

Hsu, T.-J., Raubenheimer, B., 2006. A numerical and field study on inner-surf and swash sediment transport. Cont. Shelf Res., 26, pp. 589-598 Scopus.

Hughes, M.G., Masselink, G., Brander, R.W., 1997. Flow velocity and sediment transport in the swash zone of a steep beach. Marine Geology, 138, pp. 91-103 Scopus.

Hughes, M.G., Baldock, T.E., 2004. Eulerian flow velocities in the swash zone: Field data and model predictions. J. Geophys. Res., 109, C08009 Scopus.

Hughes, M.G., Moseley, A.S., 2007. Hydrokinematic regions within the swash zone. Continental Shelf Research, 27, 2000-2013 Scopus.

Hughes, M.G., Aagaard, T., Baldock, T.E., 2007. Suspended sediment in the swash zone: Heuristic analysis of spatial and temporal variations in concentration. Journal of Coastal Research, 23, 1345-1354 Scopus.

Karambas, Th.V., 2006. Prediction of sediment transport in the swash zone by using a nonlinear wave model. Cont. Shelf Res., 26, pp. 599-609 Scopus.

Kobayashi, N., Johnson, B. D., 2001. Sand suspension, storage, advection, and settling in surf and swash zones. J. Geophys. Res., 106(C5), pp. 9363–9376 Scopus.

Kobayashi, N., Tega, Y., Hancock, M.W., 1996. Wave Reflection and Overwash of Dunes, J. Waterway, Port, Coast. and Ocean Eng., ASCE, 122(3), pp. 150-153 Scopus.

Masselink, G., Hughes, M.G., 1998. Field investigation of sediment transport in the swash zone. Cont. Shelf Res., 18, pp. 1179–1199 Scopus.

Masselink, G. & Puleo, J., 2006. Swash zone morphodynamics. Continental Shelf Research, 26(5), 661–680.

Masselink, G., Evans, D., Hughes, M.G., Russell, P. 2005. Suspended sediment transport in the swash zone of a dissipative beach. Mar. Geology, 216, pp. 169–189 Scopus.

Myrhaug, D., Holmedal, L.E., Simons, R.R., MacIver, R.D., 2001. Bottom friction in random waves plus current flow. Coastal Eng., 43, pp. 75–92 Scopus.

Nielsen, P., 1992. Coastal bottom boundary layers and sediment transport, Advanced Series on Ocean Engineering, World Scientific, Singapore, 324 pp.

Nielsen, P., 2006. Sheet flow sediment transport under waves with acceleration skewness and boundary layer streaming. Coastal Eng., 53, pp 749-758 Scopus.

Nielsen, P., Callaghan, D. P., 2003. Shear stress and sediment transport calculations for sheet flow under waves. Coastal Eng. J., 47, pp 347-354 Scopus.

Nielsen, O., Roberts, S., Gray, D., McPherson, A., Hitchman, A., 2005. Hydrodynamic modelling of coastal inundation, Proc. ModSIM, CD-ROM.

Petti, M., Longo, S., 2001. Turbulence experiments in the swash zone, Coastal Eng., 43, pp. 1–24 Scopus

Pritchard, D., Hogg, A.J., 2005. On the transport of suspended sediment by a swash event on a plane beach, Coastal Eng., 52, pp. 1–23 Scopus

Pritchard, D., Guard, P.A., Baldock, T.E., 2008. An analytical model for bore-driven run-up, J. Fluid Mechanics, *in press*.

Puleo, J. A., Holland, K.T., Plant, N.G., Slinn, D.N., Hanes, D.M., 2003. Fluid acceleration effects on suspended sediment transport in the swash zone. J. Geophys. Res., 108(C11), 3350 Scopus.

Puleo, J.A., Farhadzadeh, A., Kabayashi, N., 2007. Numerical simulation of swash zone fluid accelerations. J. Geophys. Res., 112, C07007 Scopus.

Rankin, K.L., Hires, R.I., 2000. Laboratory Measurement of Bottom Shear Stress on a Movable Bed, J. Geophys. Res., 105(C7), pp. 17011-17019 Scopus.

Raubenheimer, B., Elgar, S., Guza, R. T., 2004. Observations of swash zone velocities: A note on friction coefficients. J. of Geophys. Res., 109, C01027 Scopus.

Riedel, H.P., 1973. Direct Measurement of Bed Shear Stress Under Waves. PhD thesis, Queen's University at Kingston, Ontario, 109 pp.

Riedel, P. H., Kamphuis, J. W., 1973. A shear plate for use in oscillatory flow. J. Hyd. Res., 11, pp. 137-156 Scopus.

Rigby, T., Van Drie, R., 2008. ANUGA – A new free and open source hydrodynamic model. Proc. Water Down Under, pp. 629-638.

Schlichting, H., Gersten, K., 2000. Boudnary-Layer Theory. Springer, New York, 799 pp.

Weir, F.M., Hughes, M.G., Baldock, T.E., 2006. Beach face and berm morphodynamics fronting a coastal lagoon. Geomorphology, 82, pp. 331-346 Scopus

Yeh, H. H., Ghazali, A., Marton, I., 1989. Experimental study of bore runup, J. Fluid Mech., 206, pp. 563–578 Scopus.

Figure 1. Swash shear plate and cell cross-sectional diagrams.

Figure 2. Schematic example of pressure gradient force, F_{PG}, and shearing force, F_S, contributing to plate displacement. x is positive shoreward.

Figure 3. The UA swash rig.

Figure 4. The UQ wave flume.

Figure 5. Typical ensemble average temporal variation of swash flow surface elevation η at the seaward and landward SSP edges; total force F_T and pressure gradient force F_{PG} (note that the F_{PG} is plotted on the secondary axis that is an order of magnitude smaller than the primary axis).; and bed shear stress τ_0 (Table 1: UAR, x = 3m).

Figure 6. Measured swash flow depth h, horizontal velocity component U_x (Hondebrink, 2006), and bed shear stress τ_0, x = 2m (left panels) and x = 3m (right panels) Solid (h) and dash (U_x) lines represent modelled parameters,. UA Swash Facility, smooth beach (Table 1: UAS x = 2 and 3m).

Figure 7. UQ wave flume model verification. Ensemble average measured (symbols) and modelled (lines) swash flow depth h and corresponding modelled horizontal velocity U_x at three cross shore locations. UQ rough beach, x = 0.07, 0.87, 1.67m (Table 1: UQR020).

Figure 8. UQ wave flume model verification. Ensemble average measured (symbols) and modelled (lines) bore characteristics at three offshore locations, x = -2.68, -1.24, -0.43 (Table 1: UQS015).

Figure 9a . Dimensionless temporal variation of swash horizontal Reynolds number Re (top panel), bed shear stress τ_0 (middle panel) and friction coefficient C_f (bottom panel). C_f calculated with measured U_x (crosses) and modelled U_x (circles). UA swash experiments, smooth beach, x / R_x = 0.52 (Table 1: UAS, x = 3m). Dash-line in bottom panel is time-varying C_f predicted by Eq. 6.

Figure 9b . Dimensionless temporal variation of swash horizontal Reynolds number Re (top panel), bed shear stress τ_0 (middle panel) and friction coefficient C_f (bottom panel). C_f calculated with measured U_x (crosses) and modelled U_x (circles). UA swash experiments, . Impermeable pebble beach d_{50} = 5.7mm; x / R_x = 0.64 (Table 1: UAR, x = 3m). Dash-line in bottom panel is time-varying C_f predicted by Eq. 6 (note that the time-varying C_f truncates at $t/T \approx 0.5$ due as k_s (Eq. 7) > D_h in Eq. 6).

Figure 10a . Dimensionless temporal variation of swash horizontal Reynolds number Re (top panel), bed shear stress τ_0 (middle panel) and friction coefficient C_f (bottom panel). UQ swash experiments, sandpaper beach d_{50} = 0.2mm, x / R_x = 0.25 (Table 1: UQR022, x = 0.68m). Dash-line in bottom panel is time-varying C_f predicted by Eq. 6.

Figure 10b . Dimensionless temporal variation of swash horizontal Reynolds number Re (top panel), bed shear stress τ_0 (middle panel) and friction coefficient C_f (bottom panel).

UQ swash experiments, sandpaper beach d_{50} = 0.2mm, x / R_x = 0.83 (Table 1: UQR022, x = 2.28m). Dash-line in bottom panel is time-varying C_f predicted by Eq. 6.

Figure 11a. Dimensionless ensemble average spatial variation of maximum landward (positive) and maximum seaward (negative) bed shear stress. x/R_x<0 indicates inner surf zone measurements. Smooth marine plywood (crosses), sandpaper d_{50} = 0.2mm (diamonds). UQ swash experiments, all measurement locations.

Figure 11b. Spatial variation of swash of C_{fmax}. x/R_x<0 indicates inner surf zone measurements. C_f >0 indicates uprush, C_f <0 indicates backwash. Smooth marine plywood (crosses), d_{50} = 0.2mm (diamonds). UQ swash experiments, all measurement locations.

Figure 12a. Uprush friction factor variation with local Reynolds number, UA pebble experiments: x = 2m (down triangles); x = 3m (up triangles). Bold symbols indicate start of data set in time.

Figure 12b. Backwash friction factor variation with local Reynolds number, UA pebble beach experiment: x = 2m (down triangles); x = 3m (up triangles). Bold symbols indicate start of data set in time.

Figure 13. Fluid particle trajectories obtained from an Eulerian-Lagrangian transformation of the numerically modelled flow field. Bold solid line represents the shoreline, thin lines represent individual fluid particle trajectories. Fluid particle initial position seaward of the SWL (x = 0) indicated by the circles. UA swash simulation, smooth bed, R_x = 5.7m.

Figure 14. Measured and modelled depth and horizontal swash velocity U_x, measured bed shear stress τ_0 and calculated bed shear stress following Equation 2 with constant C_f. Dimensionless measurement location $x/R_x = 0.3$; sandpaper beach (Table 1: UQR020, $x = 0.87$m).

Figure 15. Spatial variation of $<C_f>$. $x/R_x<0$ indicates inner surf zone measurements. $<C_f> >0$ indicates uprush, $<C_f> <0$ indicates backwash. Smooth marine plywood (crosses), sandpaper $d_{50} = 0.2$mm (diamonds), smooth Perspex (squares), pebbles $d_{50} = 5.7$mm (circles), all measurement locations.

Figure 16a. Spatial variation of swash $<|\tau_0|U>$. $x/R_x<0$ indicates inner surf zone measurements. Smooth marine plywood (crosses), smooth Perspex (squares), sandpaper equivalent grainsize $d_{50} = 0.2$mm (diamonds).

Figure 16b. Spatial variation of swash $<\tau_0 U^2>$. $x/R_x<0$ indicates inner surf zone measurements. Smooth marine plywood (crosses), smooth Perspex (squares), sandpaper equivalent grainsize $d_{50} = 0.2$mm (diamonds).

Figure 16c. Spatial variation of swash $<\tau_0 U^2 h>$. $x/R_x<0$ indicates inner surf zone measurements. Smooth marine plywood (crosses), smooth Perspex (squares), sandpaper equivalent grainsize $d_{50} = 0.2$mm (diamonds).

1

2

3 Table 1. Experiments summary.

Experiement	Name	Beach material	Offshore depth [m]	Cross-shore measurement locations, relative to SWL [m]	R_x [m]
UA swash smooth beach	UAS	Perspex	0.06	2 & 3	5.72
UA swash rough beach	UAR	Fixed pebble, d_{50} = 5.8mm	0.06	2 & 3	4.67
UQ swash smooth beach	UQS015	Marine plywood	0.15	0.69 & 1.49	2.4
	UQS020		0.2	0.07, 0.87, 1.67	2.8
	UQS022		0.22	-0.12, 0.68, 1.48	2.99
UQ swash rough beach	UQR015	Sandpaper, d_{50} = 0.2mm	0.15	0.69 & 1.49	2.35
	UQR020		0.2	0.07, 0.87, 1.67, 2.47	2.72
	UQR022		0.22	-0.12, 0.68, 1.48, 2.28	2.75

4

Figure_1

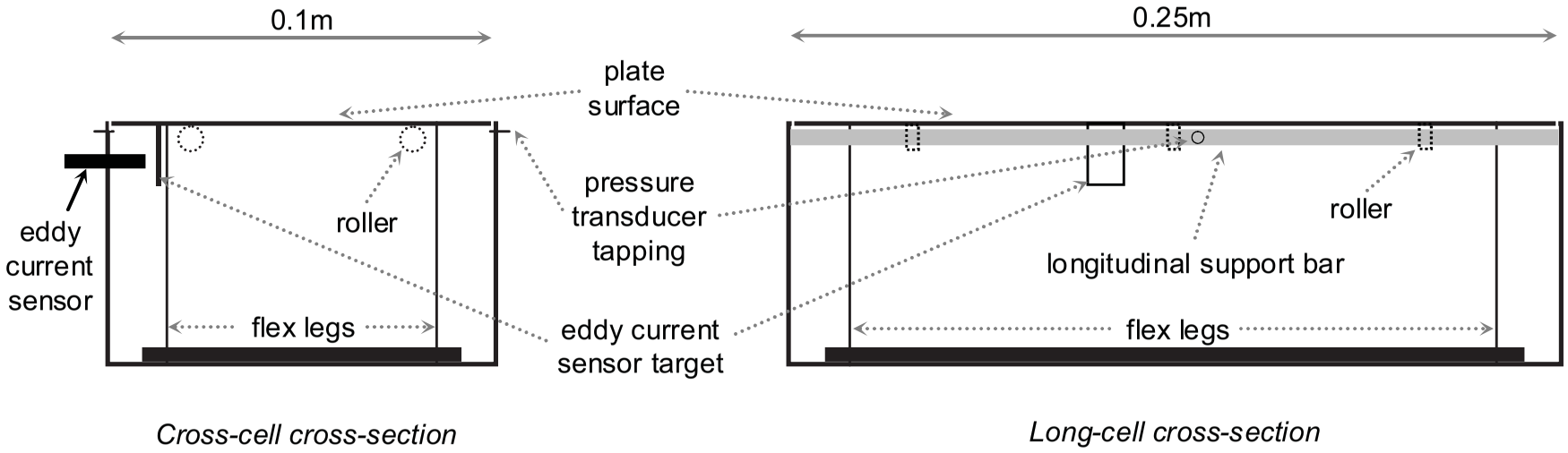
0.1m
0.25m
plate
surface
pressure
transducer
tapping
eddy
current
sensor
roller
flex legs
eddy current
sensor target
roller
longitudinal support bar
flex legs
Cross-cell cross-section
Long-cell cross-section

Figure_2

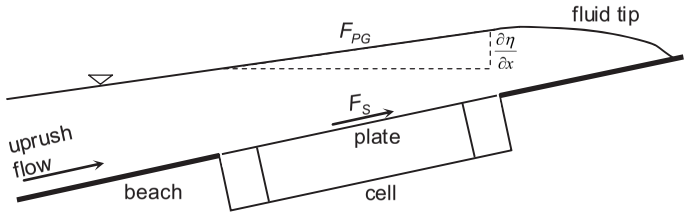
fluid tip
F_{PG}
$\frac{\partial \eta}{\partial x}$
F_S
plate
uprush
flow
beach
cell

Figure_3

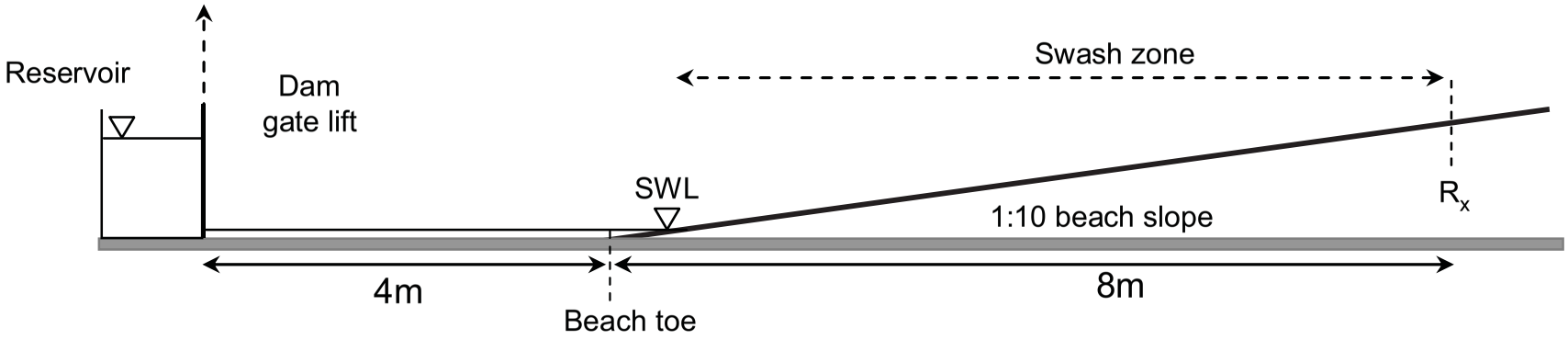
Reservoir
Dam
gate lift
Swash zone
SWL
R_x
1:10 beach slope
4m
8m
Beach toe

Figure_4

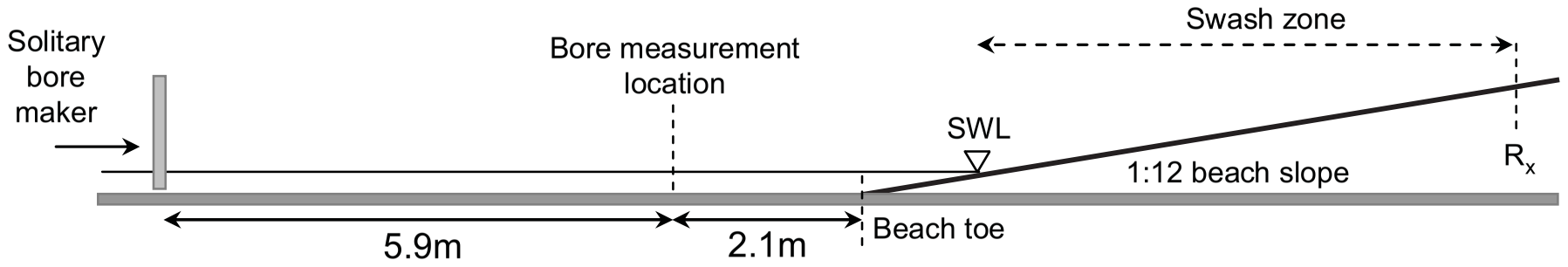
Solitary
bore
maker
Bore measurement
location
Swash zone
SWL
1:12 beach slope
R_x
5.9m
2.1m
Beach toe

Figure_5

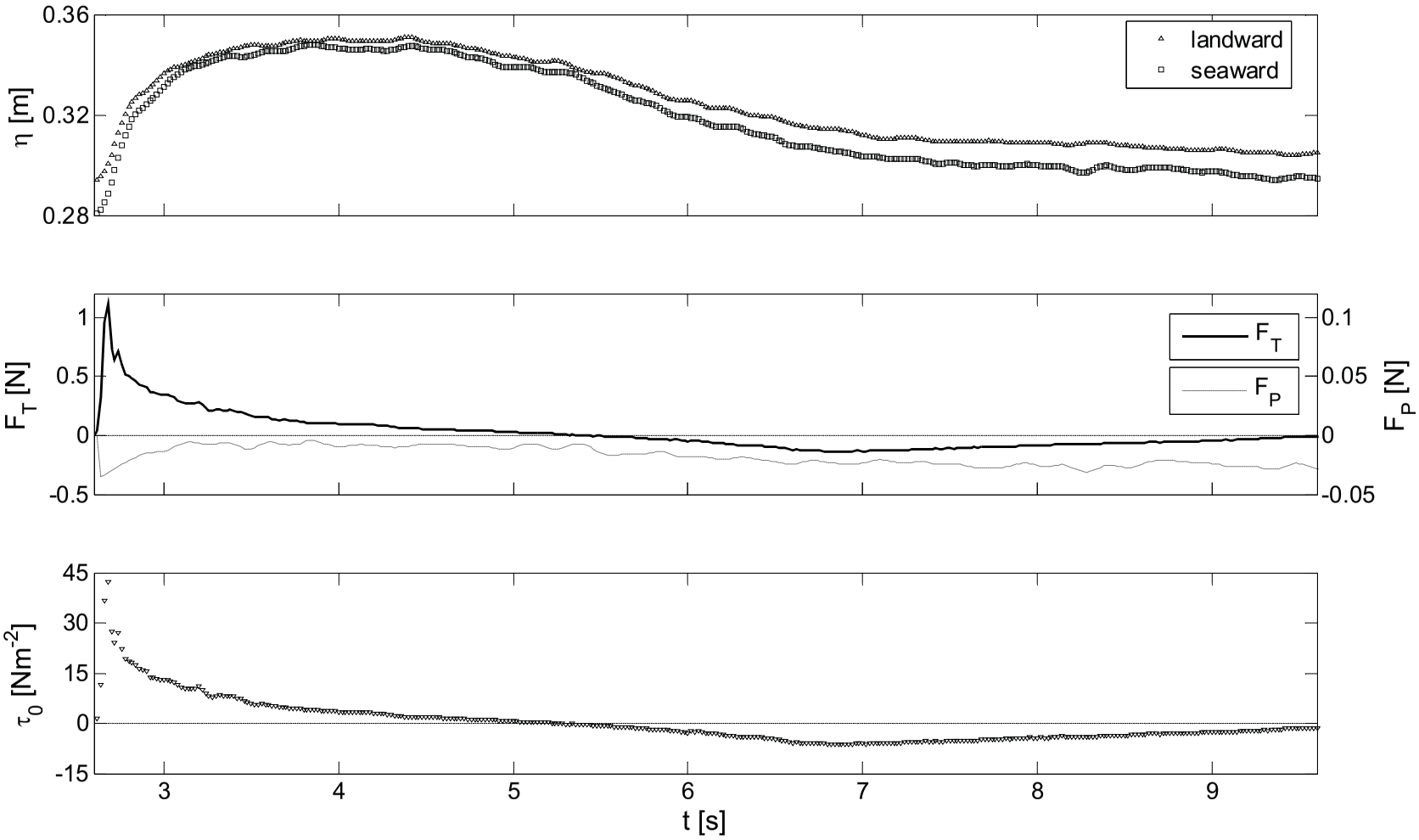
0.36
0.32
0.28
η [m]
landward
seaward
1
0.5
0
-0.5
F_T [N]
F_T
F_P
0.1
0.05
0
-0.05
F_P [N]
45
30
15
0
-15
τ_0 [Nm^-2]
3
4
5
6
7
8
9
t [s]

Figure_6

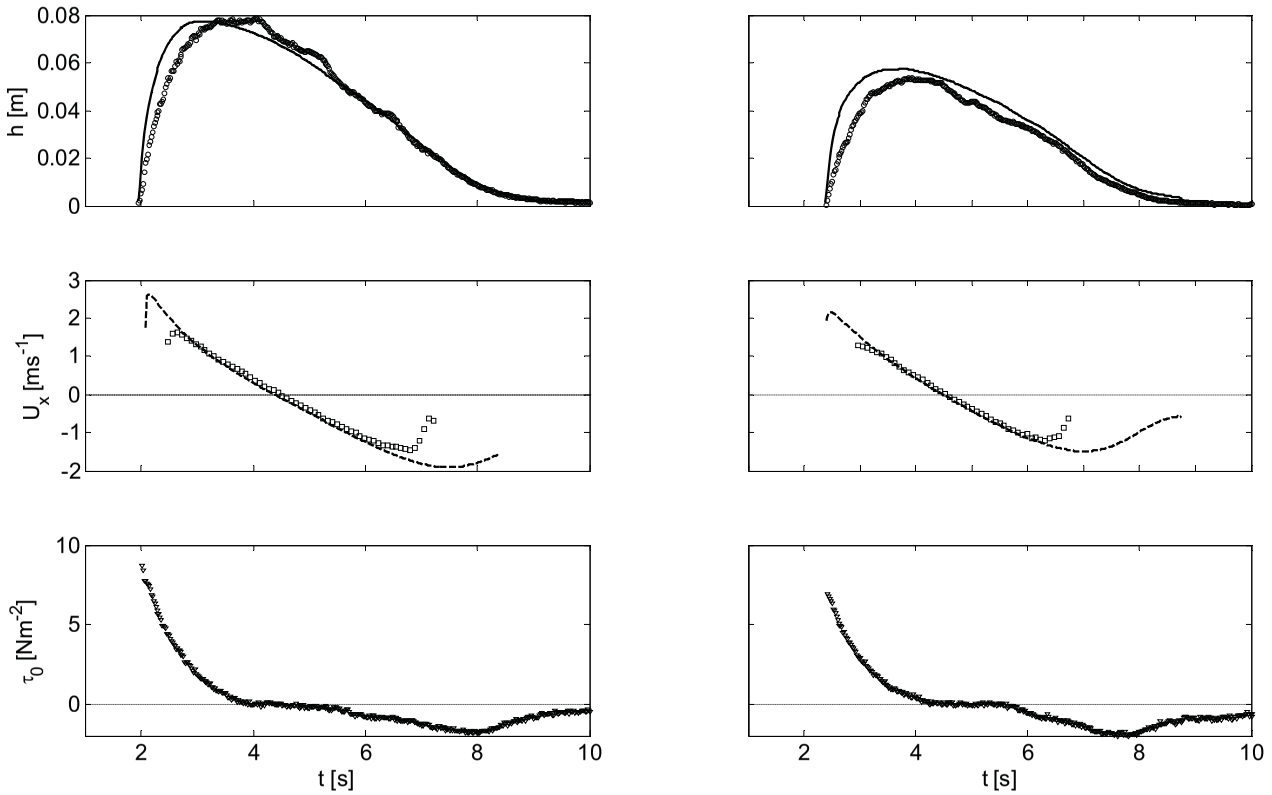
h [m]
0.08
0.06
0.04
0.02
0
U_x [ms^{-1}]
3
2
1
0
-1
-2
τ_0 [Nm^{-2}]
10
5
0
2
4
6
8
10
t [s]
2
4
6
8
10
t [s]

Figure_7

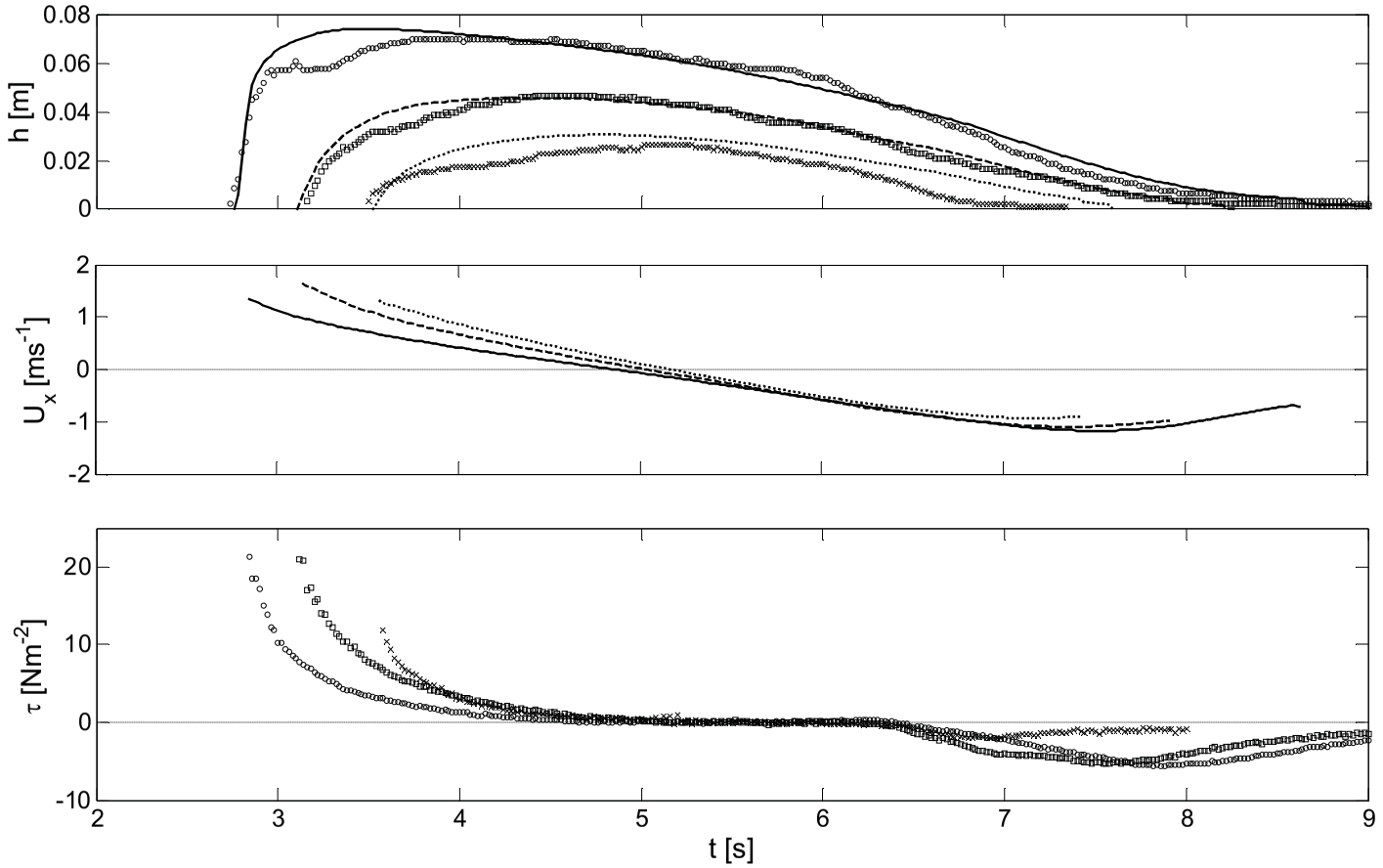

Figure_8

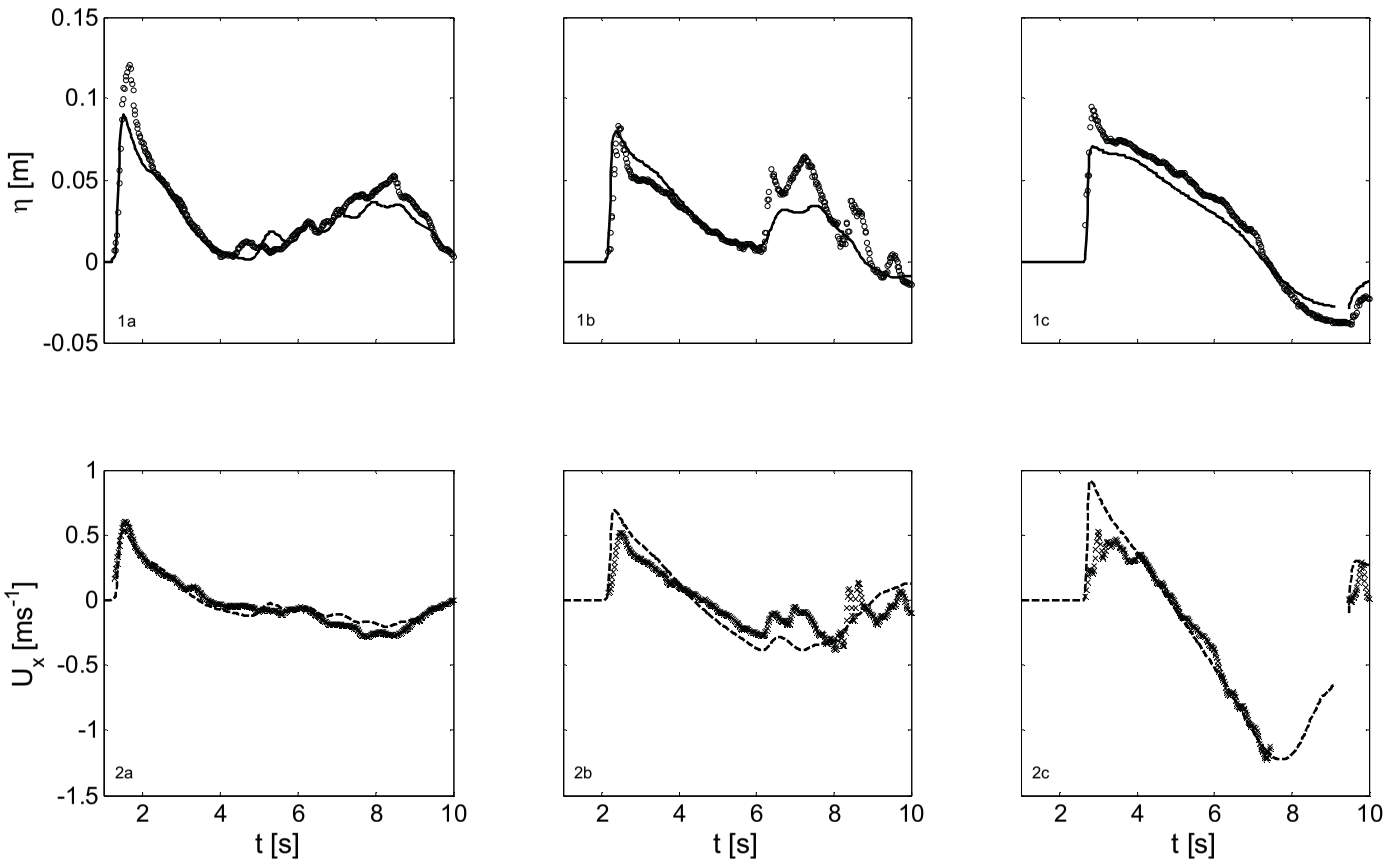

Figure_9a

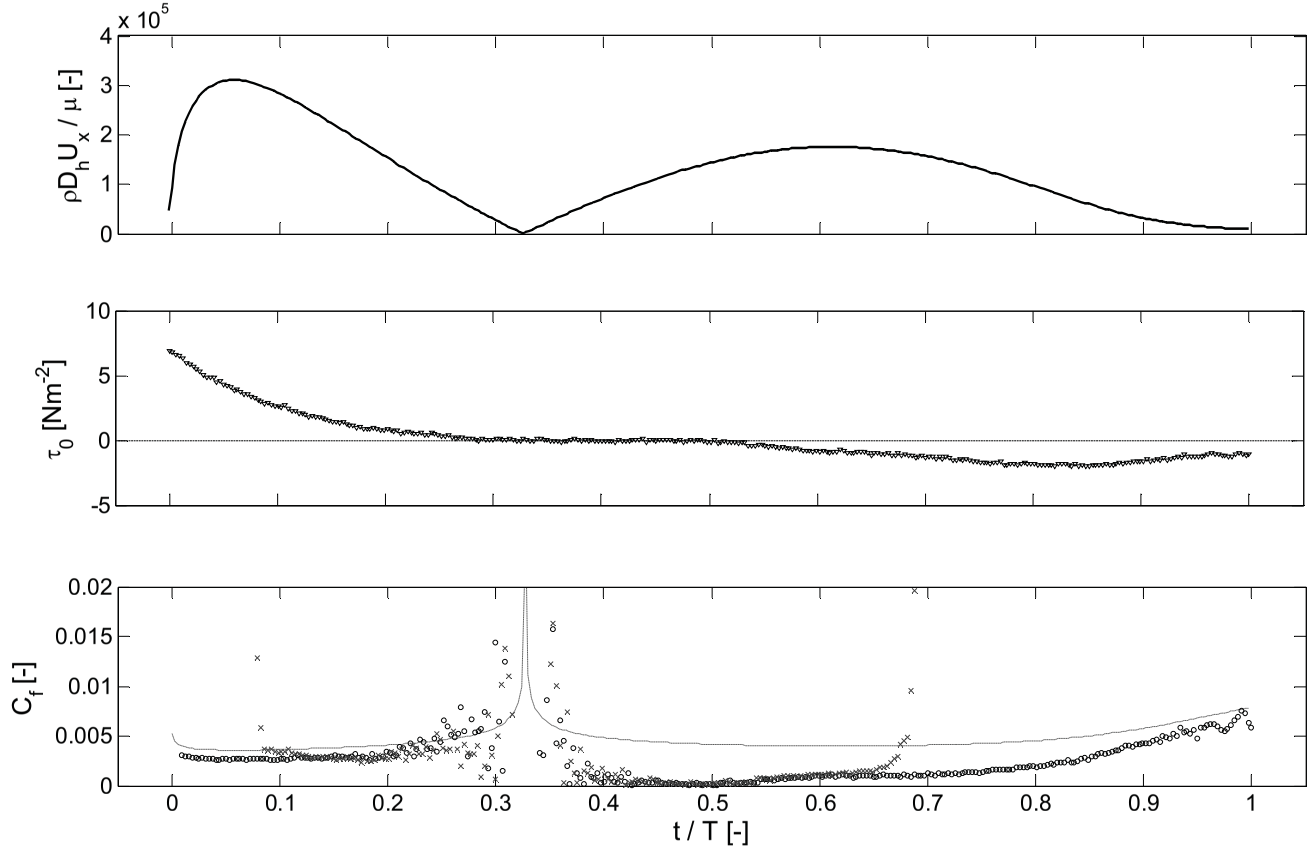
x 10^5
4
3
2
1
0
ρD_h U_x / μ [-]
10
5
0
-5
τ_0 [Nm^-2]
0.02
0.015
0.01
0.005
0
C_f [-]
0
0.1
0.2
0.3
0.4
0.5
0.6
0.7
0.8
0.9
1
t / T [-]

Figure_9b

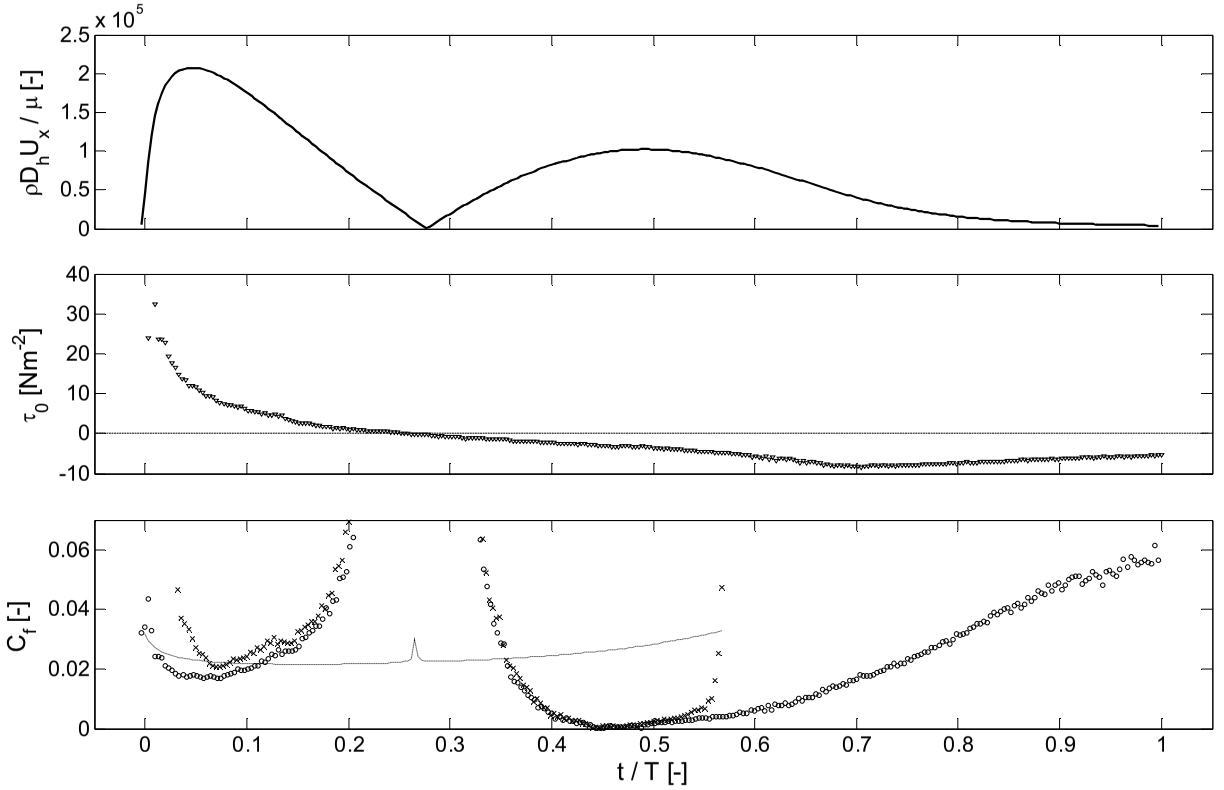
x 10^5
2.5
2
1.5
1
0.5
0
ρD_h U_x / μ [-]
40
30
20
10
0
-10
τ_0 [Nm^-2]
0.06
0.04
0.02
0
C_f [-]
0
0.1
0.2
0.3
0.4
0.5
0.6
0.7
0.8
0.9
1
t / T [-]

Figure_10a

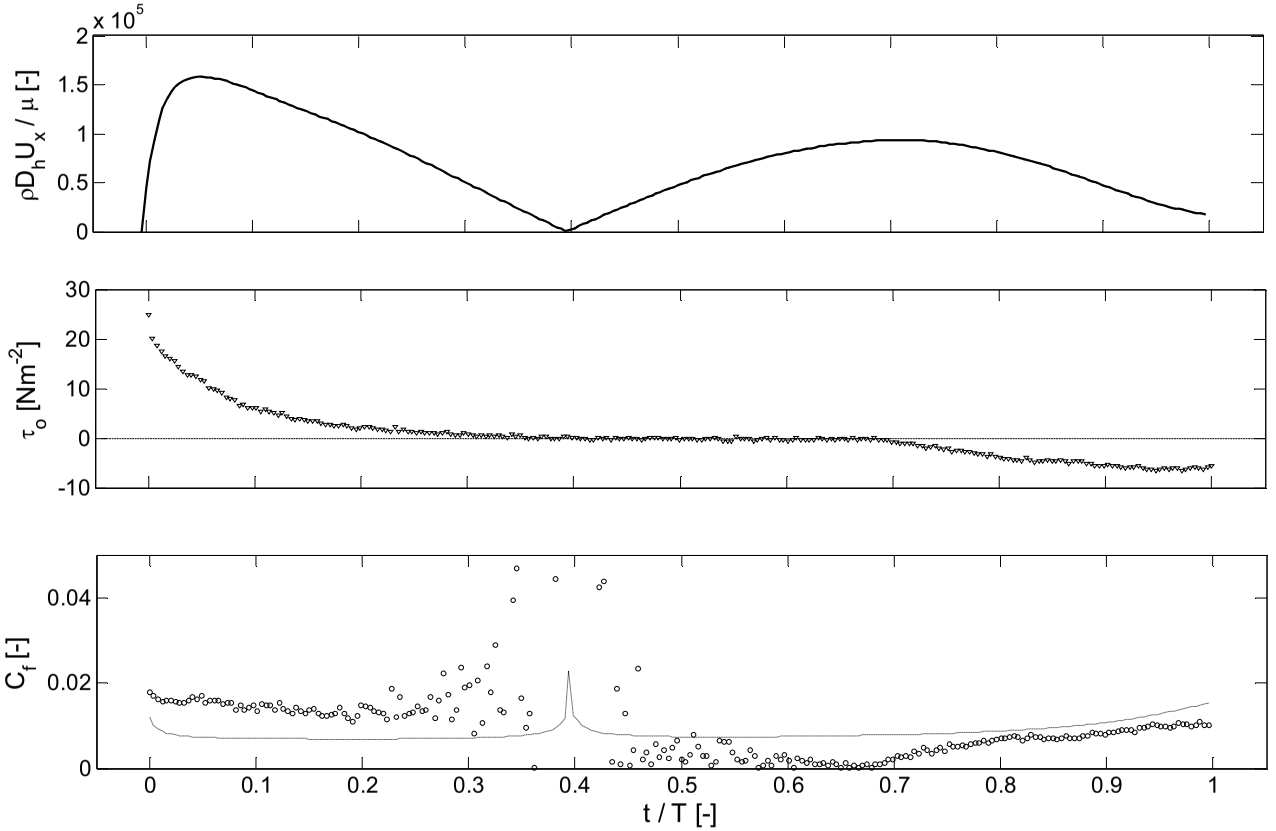
x 10^5
2
1.5
1
0.5
0
ρD_h U_x / μ [-]
30
20
10
0
-10
τ_o [Nm^-2]
0.04
0.02
0
C_f [-]
0
0.1
0.2
0.3
0.4
0.5
0.6
0.7
0.8
0.9
1
t / T [-]

Figure_10b

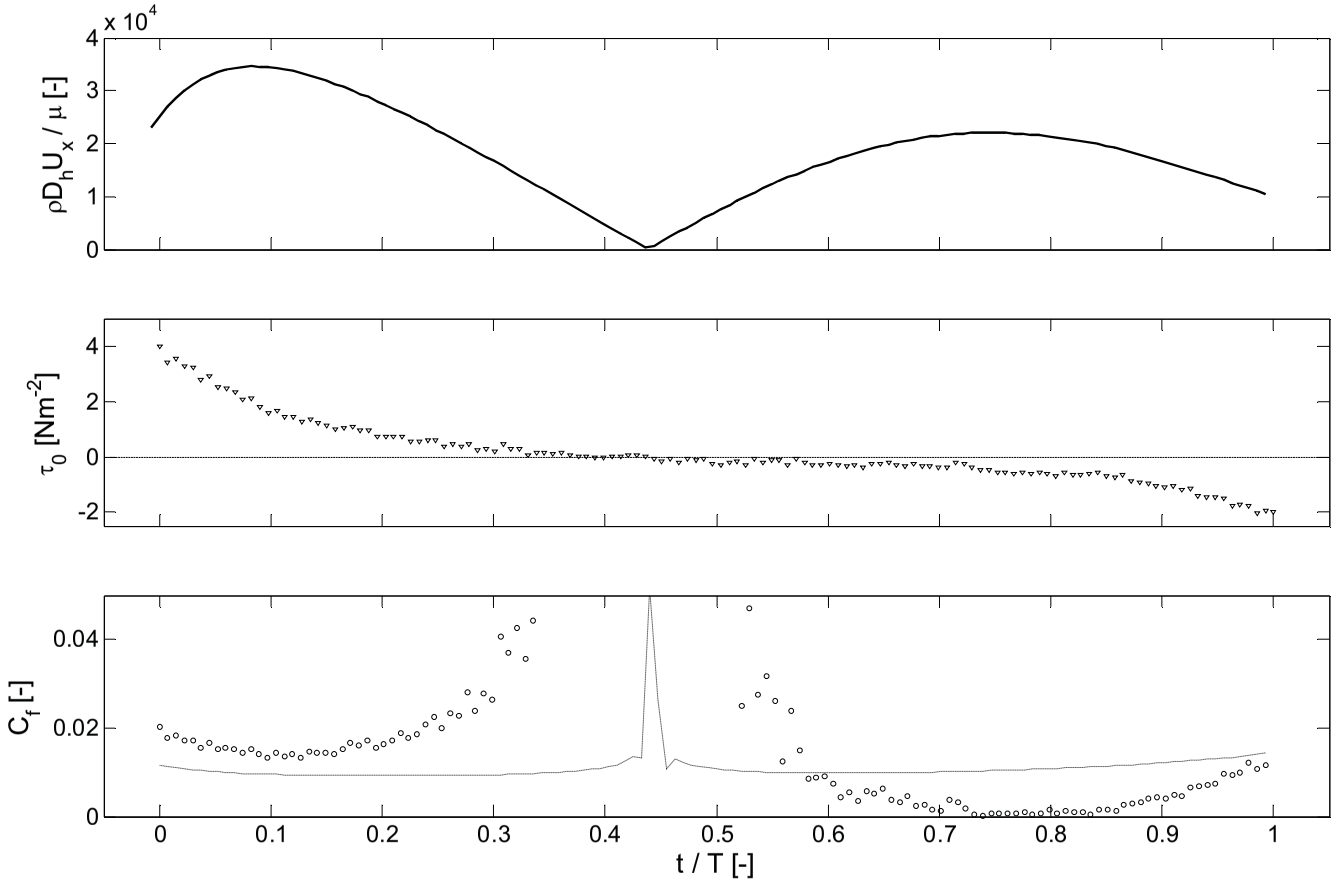

Figure_11a

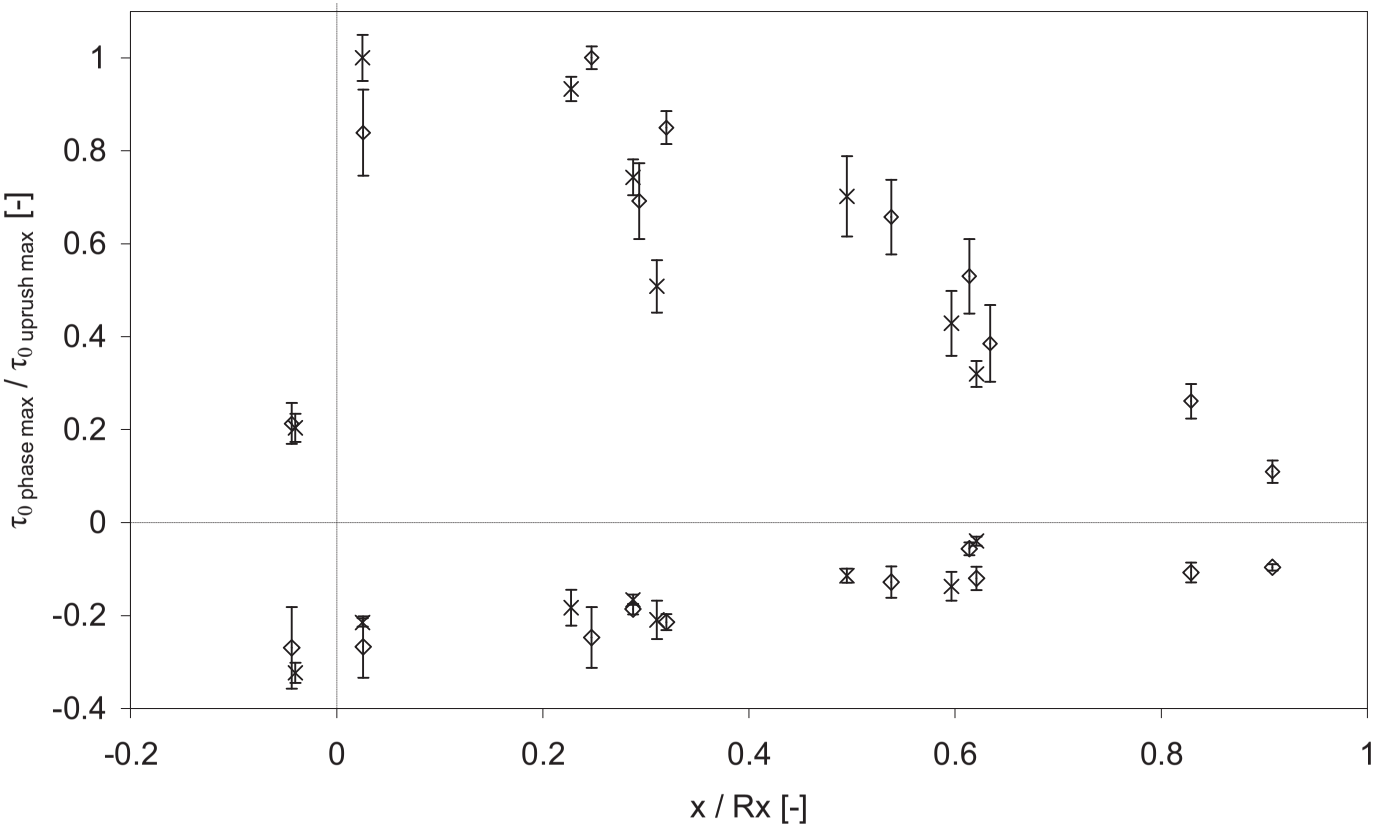
1
0.8
0.6
0.4
0.2
0
-0.2
-0.4
-0.2
0
0.2
0.4
0.6
0.8
1
τ0 phase max / τ0 uprush max [-]
x / Rx [-]

Figure_11b

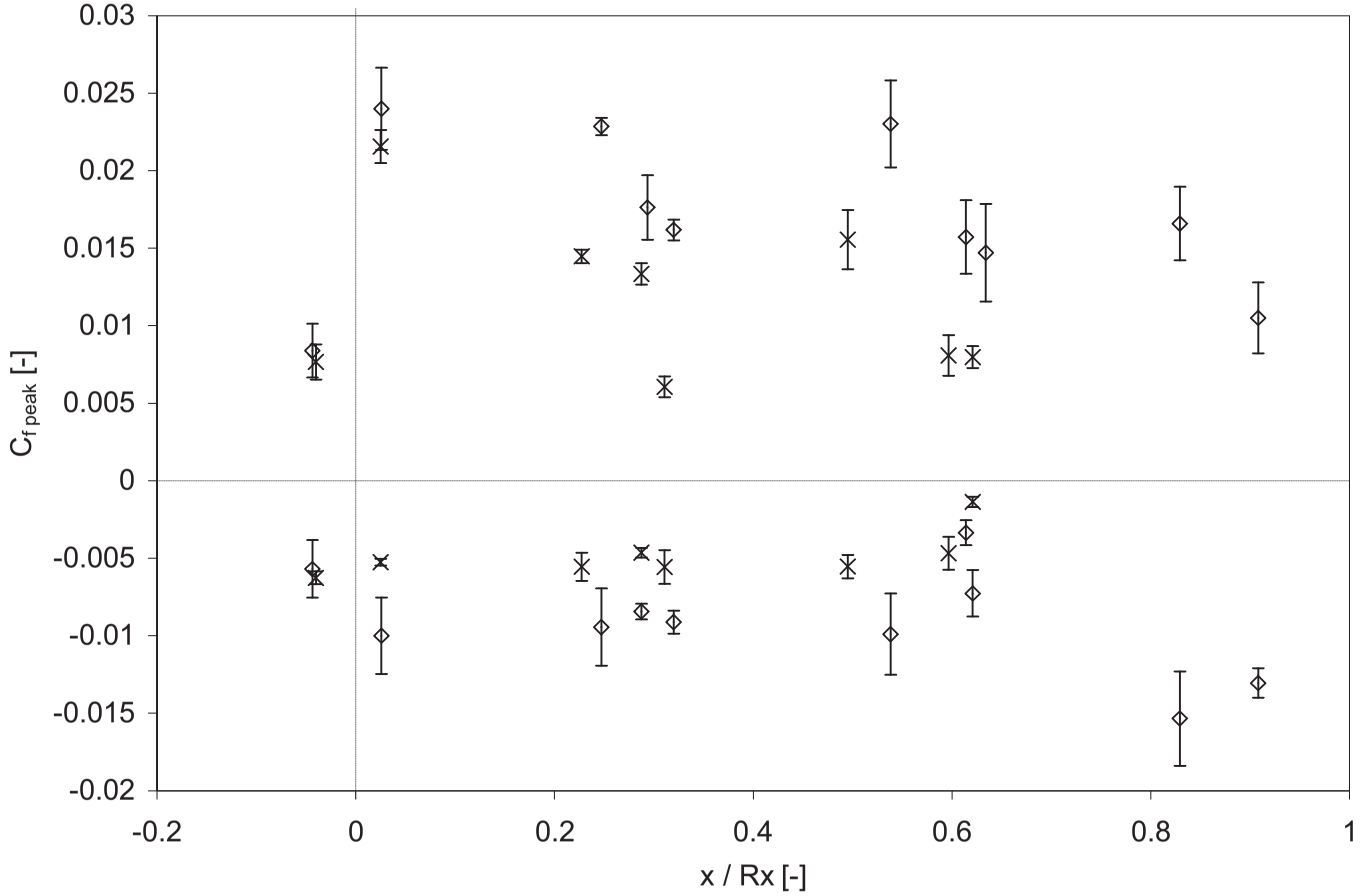
0.03
0.025
0.02
0.015
0.01
0.005
0
-0.005
-0.01
-0.015
-0.02
$C_{f\,peak}$ [-]
-0.2
0
0.2
0.4
0.6
0.8
1
x / Rx [-]

Figure_12a

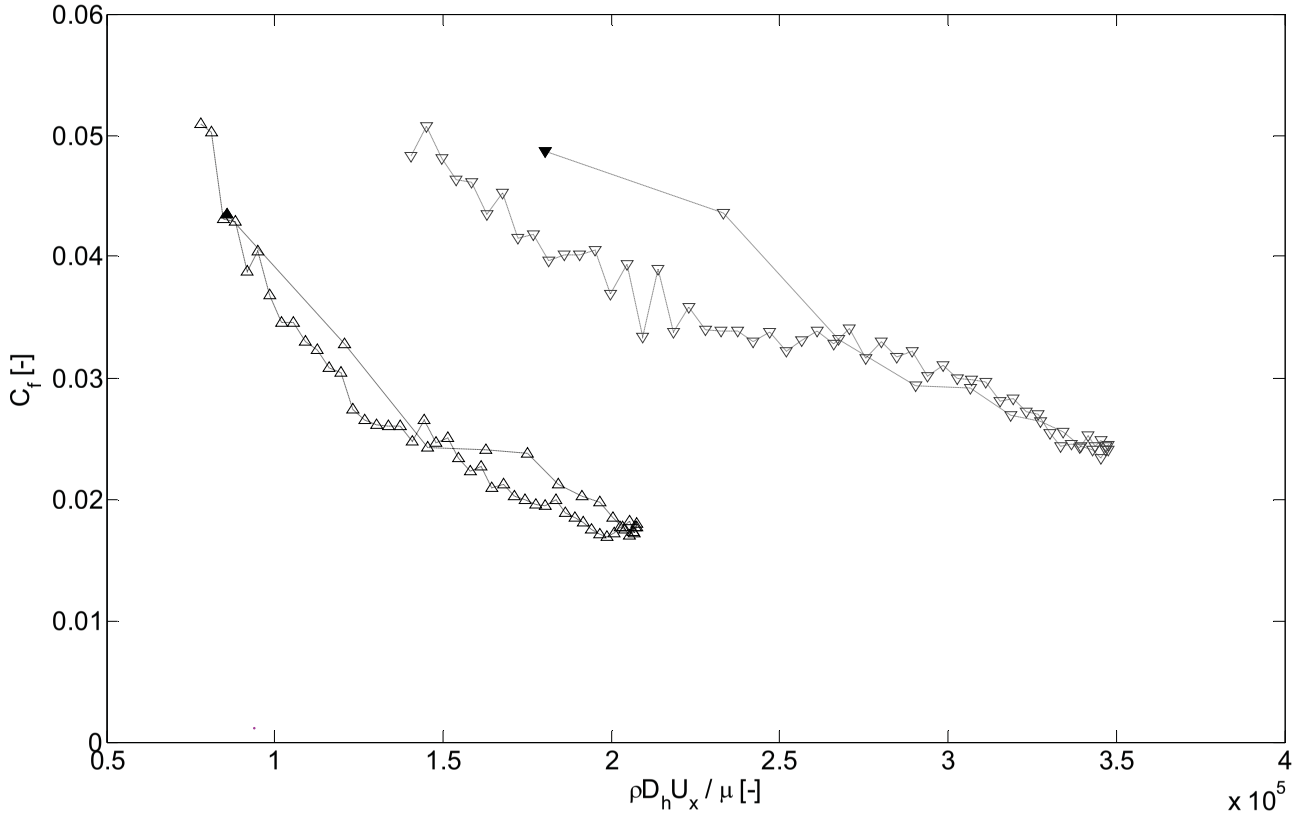

Figure_12b

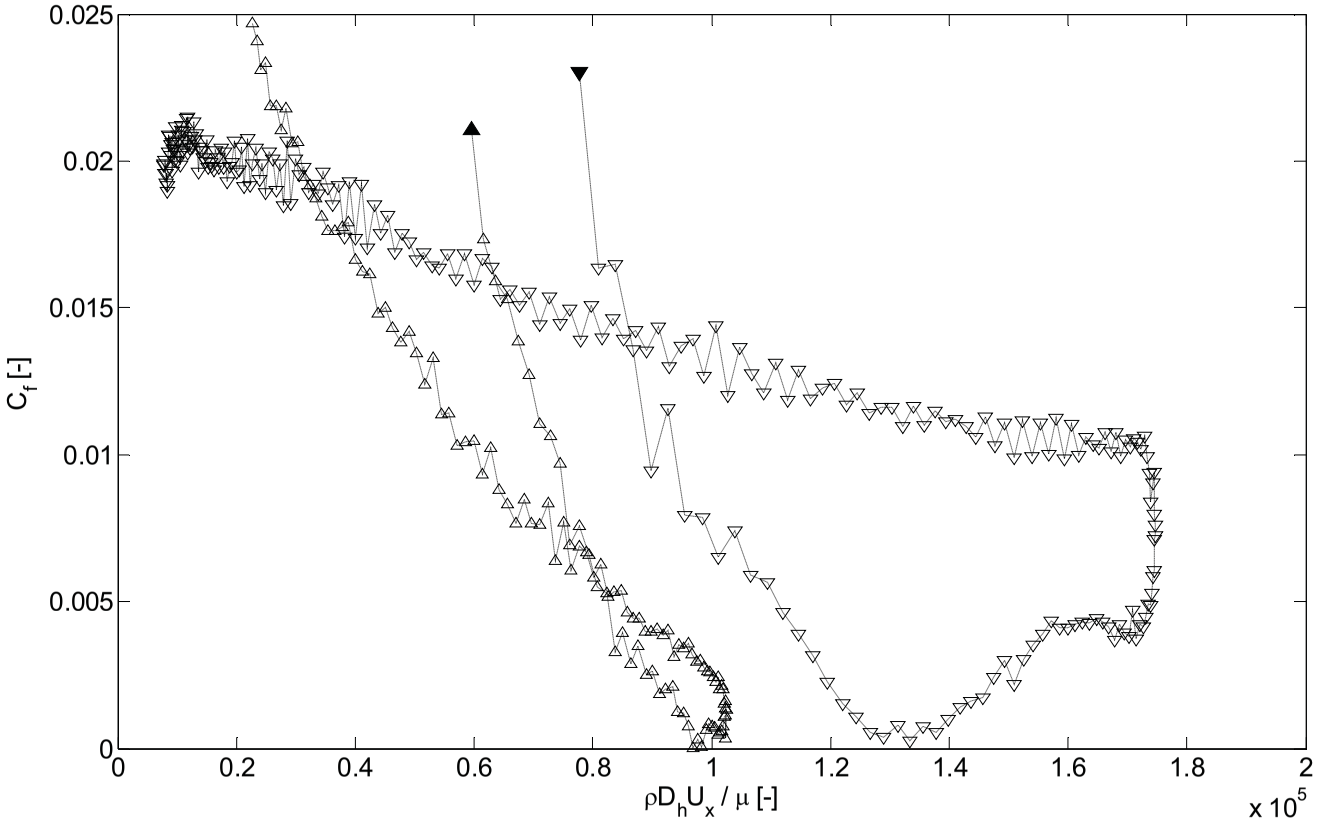
0.025
0.02
0.015
0.01
0.005
0
C_f [-]
0
0.2
0.4
0.6
0.8
1
1.2
1.4
1.6
1.8
2
$\rho D_h U_x / \mu$ [-]
x 10^5

Figure_13

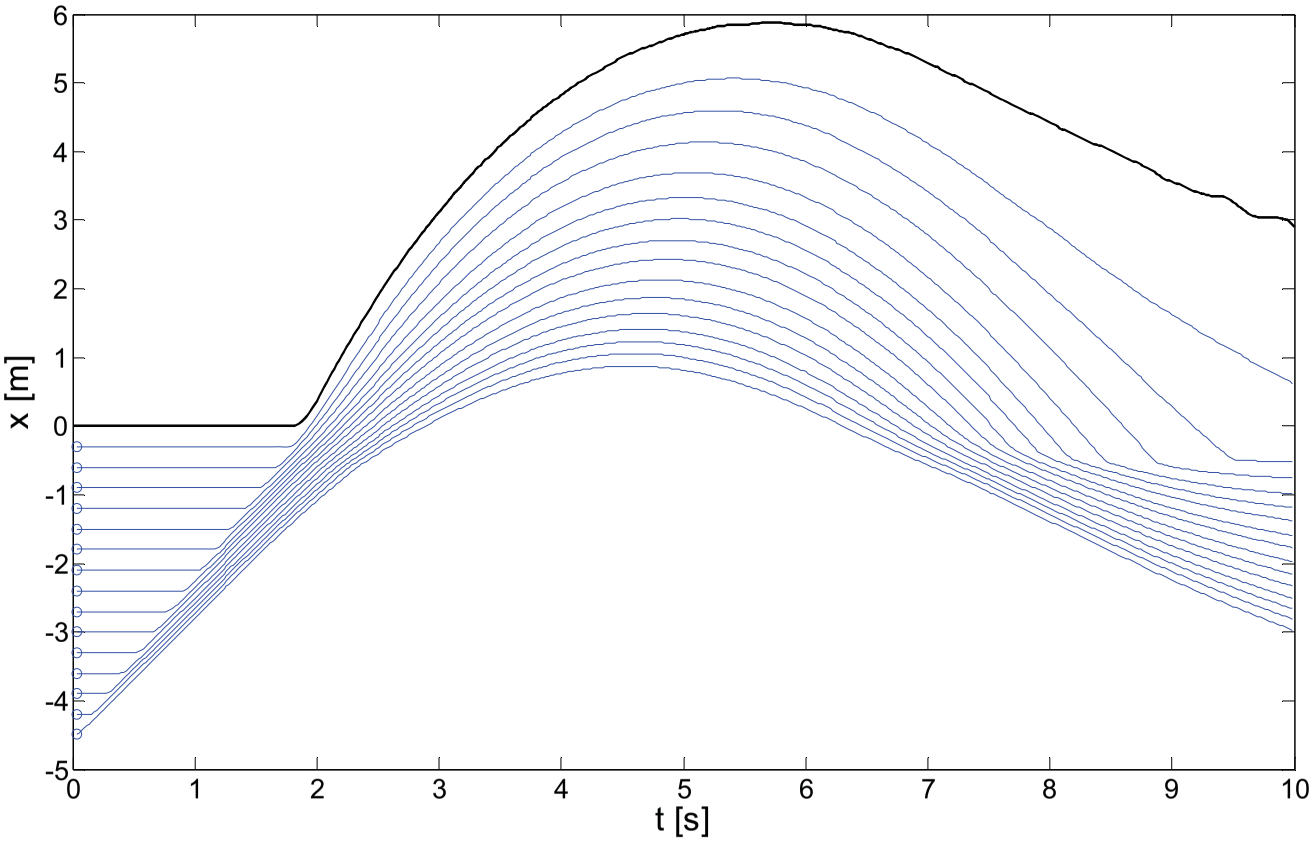

Figure_14

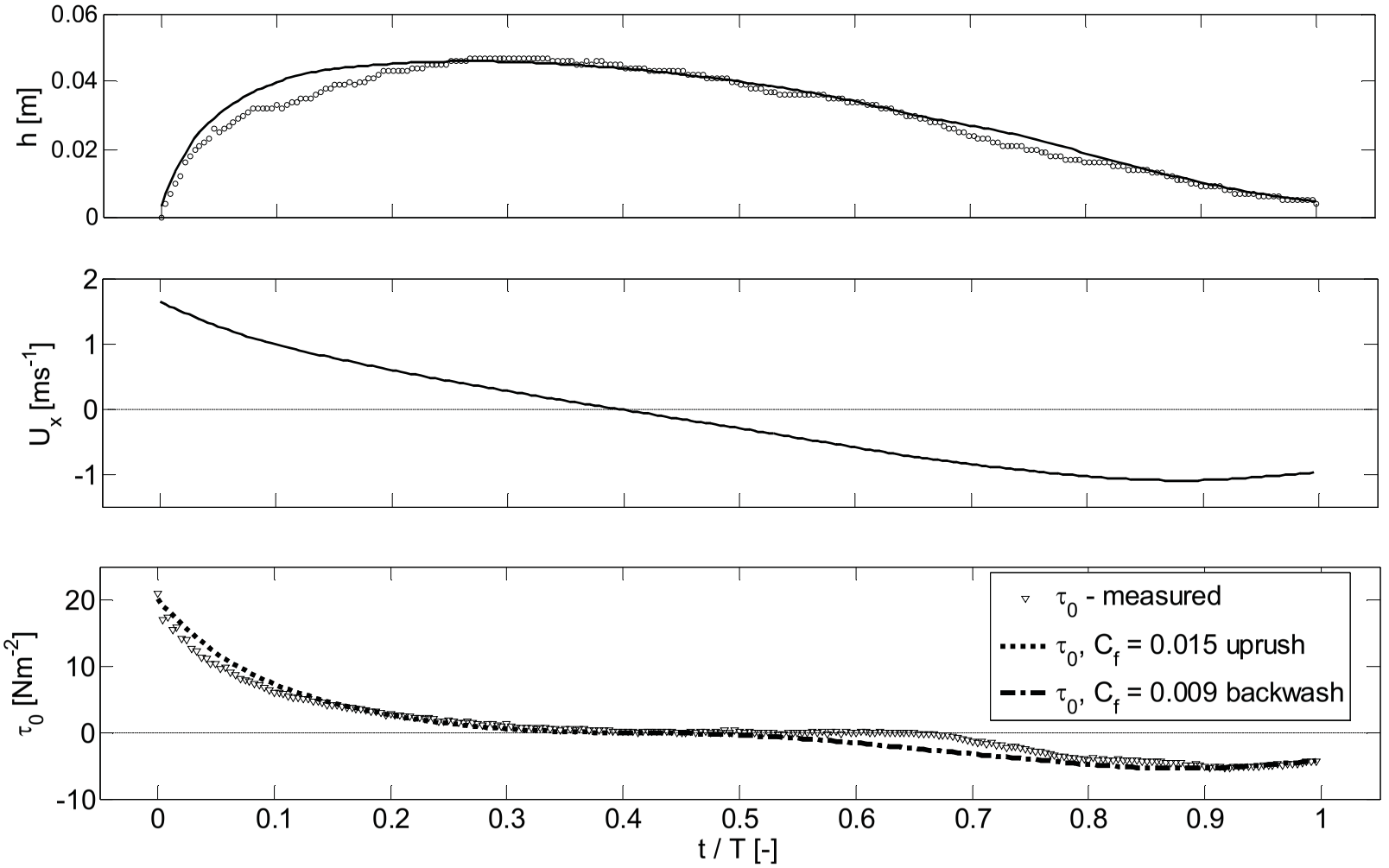
0.06
0.04
0.02
0
h [m]
2
1
0
-1
U_x [ms^{-1}]
20
10
0
-10
τ_0 [Nm^{-2}]
τ_0 - measured
τ_0, C_f = 0.015 uprush
τ_0, C_f = 0.009 backwash
0
0.1
0.2
0.3
0.4
0.5
0.6
0.7
0.8
0.9
1
t / T [-]

Figure_15

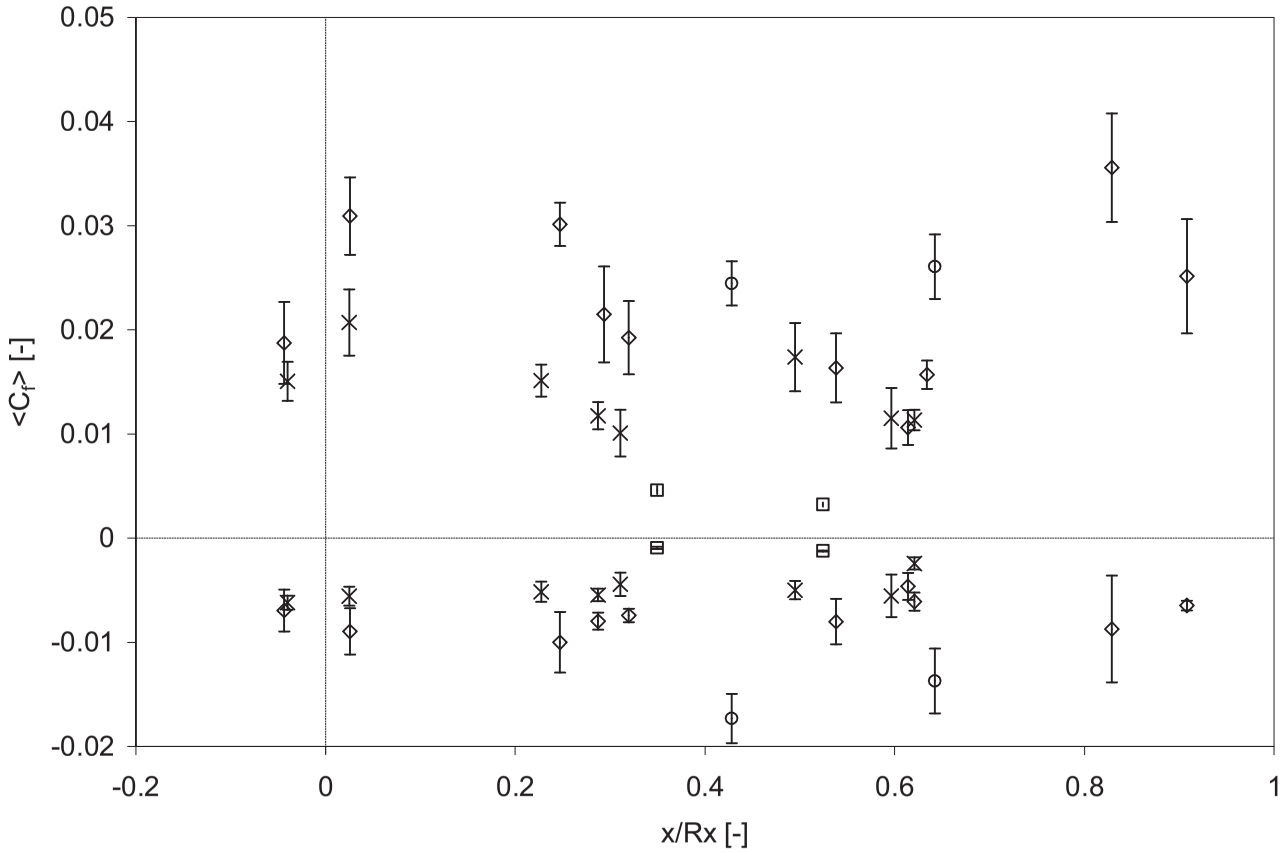

Figure_16a

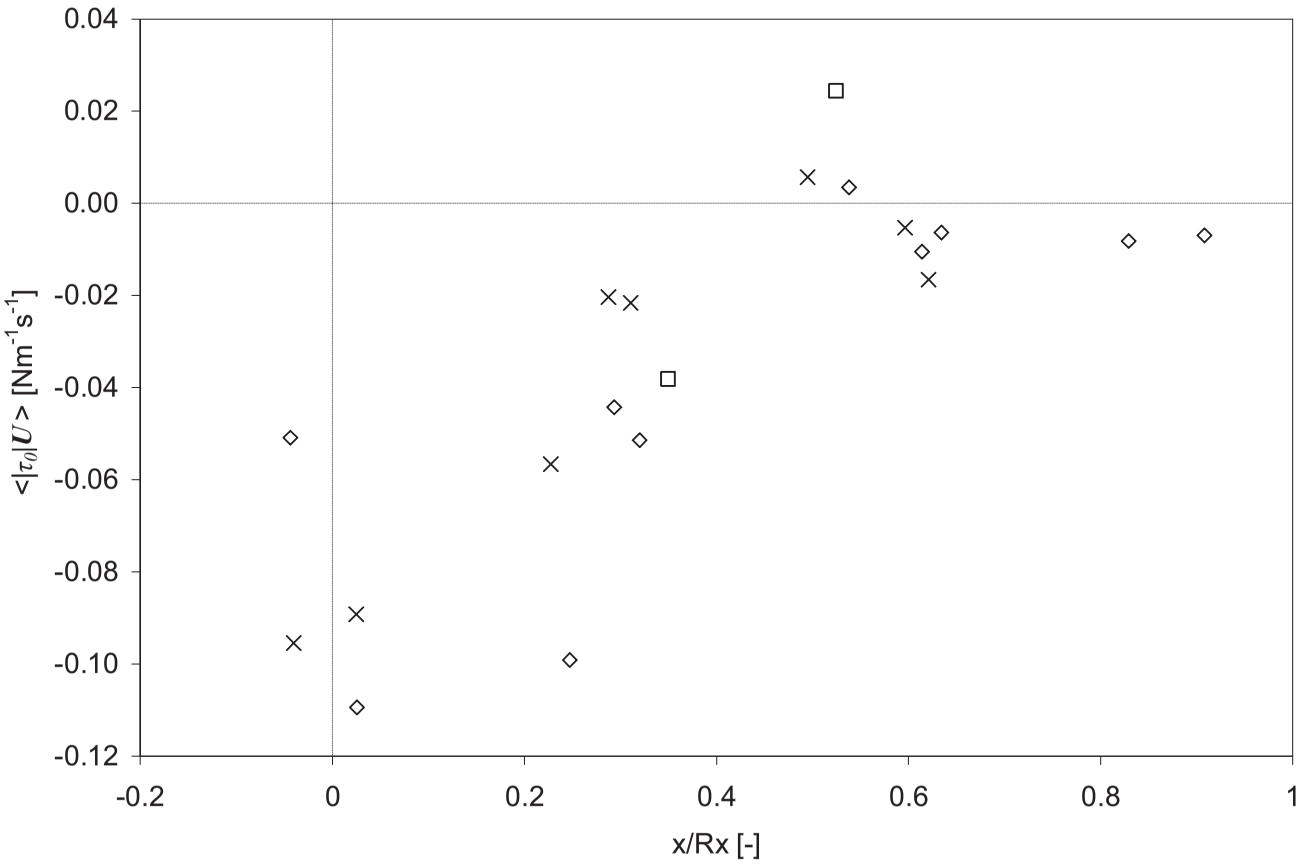
0.04
0.02
0.00
-0.02
-0.04
-0.06
-0.08
-0.10
-0.12
-0.2
0
0.2
0.4
0.6
0.8
1
x/Rx [-]
<|τ0|U> [Nm-1s-1]

Figure_16b

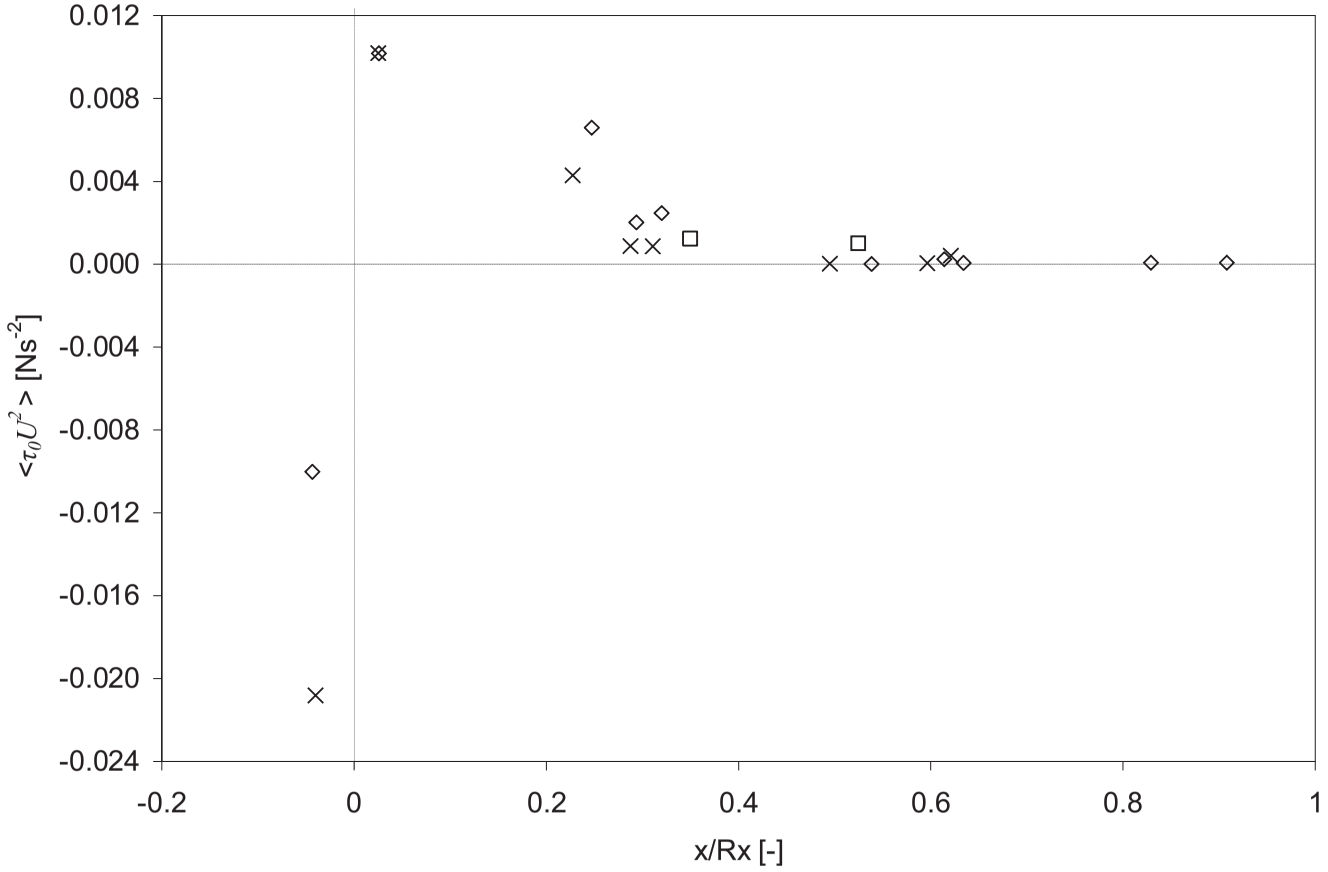
0.012
0.008
0.004
0.000
-0.004
-0.008
-0.012
-0.016
-0.020
-0.024
-0.2
0
0.2
0.4
0.6
0.8
1
x/Rx [-]
<τ0U2> [Ns-2]

Figure_16c

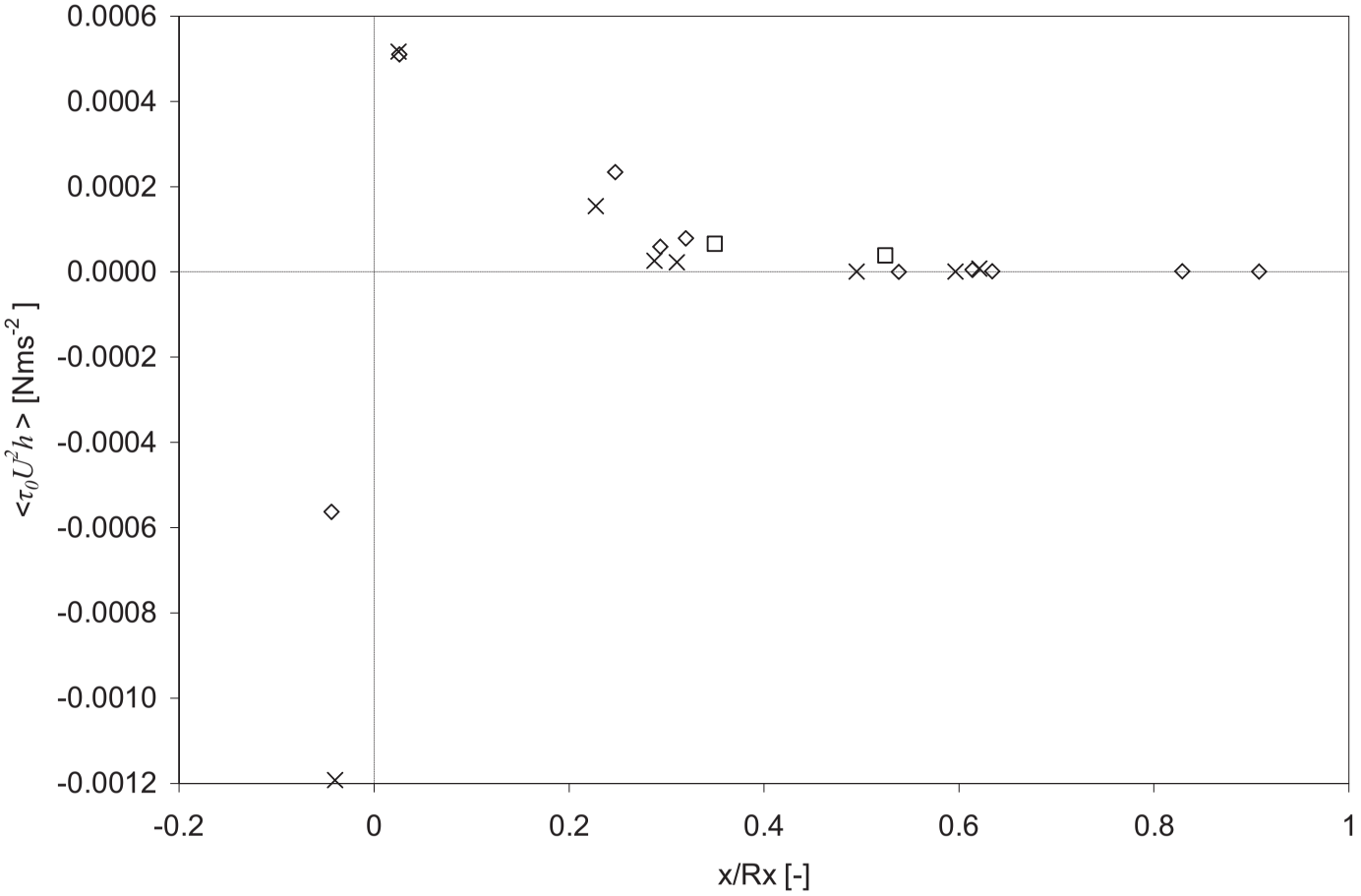
0.0006
0.0004
0.0002
0.0000
-0.0002
-0.0004
-0.0006
-0.0008
-0.0010
-0.0012
-0.2
0
0.2
0.4
0.6
0.8
1
x/Rx [-]
<τ0U²h> [Nms-2]

Table

Experiement	Name	Beach material	Offshore depth [m]	Cross-shore measurement locations, relative to SWL [m]	R_x [m]
UA swash smooth beach	UAS	Perspex	0.06	2 & 3	5.72
UA swash rough beach	UAR	Fixed pebble, d_{50} = 5.8mm	0.06	2 & 3	4.67
UQ swash smooth beach	UQS015	Marine plywood	0.15	0.69 & 1.49	2.4
	UQS020		0.2	0.07, 0.87, 1.67	2.8
	UQS022		0.22	-0.12, 0.68, 1.48	2.99
UQ swash rough beach	UQR015	Sandpaper, d_{50} = 0.2mm	0.15	0.69 & 1.49	2.35
	UQR020		0.2	0.07, 0.87, 1.67, 2.47	2.72
	UQR022		0.22	-0.12, 0.68, 1.48, 2.28	2.75